UNIVERSITÀ DEGLI STUDI DI MILANO

Corso di dottorato in BIOLOGIA MOLECOLARE E CELLULARE
XXXIV cycle

Dipartimento di Bioscienze

TESI DI DOTTORATO DI RICERCA

Transmembrane chloride intracellular channel 1 (tmCLIC1) protein is a key regulator of colorectal cancer's proliferation and metastasis

FRANCESCA CIANCI
Matricola: R12269

TUTOR: Prof. Michele Mazzanti, PhD

A.A. 2020/2021

Abstract

Colorectal cancer is the third leading cause of death in developed countries. Although the huge progresses reached in therapeutical approach, in the presence of metastasis colorectal cancer remains still uncurable. Ion channels have a prominent role in the acquirement of aggressive phenotype, and they are considered the ideal target to design an anticancer therapy. The main problem is that most of them are involved in normal physiological processes and treatments against their activity could result in high toxicity.

From several years, our laboratory has focused its attention on the study of CLIC1 protein, considered a promising candidate for a targeted anticancer adjuvant therapy. CLIC1 is a ubiquitous protein belonging to a partially unexplored protein family, the CLICs, that have the peculiar characteristic to be metamorphic. In normal conditions, CLIC1 protein is expressed by all cell types as a cytosolic monomer. Upon stress stimuli, monomers undergo a conformational change and translocate to the plasma membrane where increase chloride permeability. CLIC1 protein was found to be overexpressed in different pathological states, including cancer, but the mechanism in tumorigenesis is still unclear.

Our laboratory has demonstrated that in glioblastoma stem cells tmCLIC1 is chronically expressed and here has a pivotal role in tumorigenesis and cancer development. CLIC1 mRNA overexpression was identified in colorectal cancer cells and is related to a poor prognosis. In this scenario, the main aim of the present work is to understand the role of tmCLIC1 in tumorigenesis, invasion, and migration potential of colorectal cancer.

To this purpose, were chosen different human immortalized colorectal cancer cells at different stage of aggressiveness according to the Dukes' classification; a method that categorizes tumor development based of the invasion of tissues and mucosa. Here, was investigated the level of expression of CLIC1 protein and the activity of its transmembrane form as an ion channel. Our results have demonstrated that tmCLIC1 protein activity is proportional to the level of aggressiveness of cells. We evaluated the effect on cellular proliferation, migration and invasion of the specific inhibitor of tmCLIC1, IAA94, and a monoclonal antibody, designed in our laboratory and made to specifically recognized the NH_2 terminal domain of CLIC1, exposed to extracellular space when the protein is docked in membrane. IAA94 and our antibody, now under license and named tmCLIC1omab, have demonstrated the same inhibitory proprieties. tmCLIC1omab could represent a good alternative for an adjuvant therapy to impair tmCLIC1 activity, considering the high toxicity *in vivo* of IAA94.

Our results have demonstrated that the inhibition of tmCLIC1 activity results in a downregulation of proliferation in the most aggressive cell lines in 2D model, as well as in 3D models. Moreover, the migration and invasion potential of colorectal cancer cells is mainly abolished when tmCLIC1 is impaired. To demonstrate that the effects observed in the presence of tmCLIC1 inhibitors are due to a specific action of the drugs on the protein, and not for the presence of other off targets, we established stable cell lines in which CLIC1 was knocked down after a lentiviral infection. Results obtained in silenced cells have demonstrated the same phenotype of cells treated with IAA94 and tmCLIC1omab.

The role of tmCLIC1 activity in tumorigenesis and cancer development was confirmed also in *in vivo* models. Experiments performed in Zebrafish embryos and immunodeficient mice have demonstrated that the silencing of CLIC1 results in the impairment of primary tumor development and formation of distal metastases. Experiments were also replicated in immunocompetent mice injected with murine colorectal cancer cells that have shown the same phenotype of human colorectal cancer cells used for all the previous trials. Our preliminary experiments have demonstrated that murine colorectal cancer cell line in which CLIC1 protein was silenced were not able to form tumors in the major part of the cases.

We tried to investigate the alteration of metastatic pathways after CLIC1 silencing. We obtained that many different genes are downregulated when CLIC1 protein is absent; in particular, genes regulated by Reactive Species of Oxygen (ROS). In this scenario, we tried to define a mechanism of action in which CLIC1 is involved.

Altogether, all the results obtained in the present work could be considered a starting point to design a new therapeutic strategy to counteract against metastatic colorectal cancer.

Moreover, if our hypothesis of tmCLIC1 mechanism of action will be confirmed and conserved in solid tumors, could represent a new milestone in anticancer research.

1. Introduction

1.1 Colorectal cancer

Colorectal cancer (CRC) is the third most diffused cancer type worldwide and the leading cause of cancer death. Sporadic CRC, caused by somatic mutations, account about 70% of all CRCs. Familiar CRCs, in which members of the same family present the predisposition to develop cancer, are about 10-30%, whereas hereditary diseases, due to the presence of a specific mutation that is hereditarian, are about 5-7% Burt [1]. In 1990, was proposed a model whereby CRCs proceed through a series of morphological modifications due to specific genetic alterations [2]. Epithelial cells of gastrointestinal trait acquire, during carcinogenesis, sequential mutations in specific oncogenes and/or tumour suppressor genes causing CRC onset, progression, and metastasis [3] (Figure 1). Three different pathogenetic pathways are involved in the development of these tumors: (1) chromosomal instability (CIN); (2) microsatellite instability (MSI); (3) CpG island methylator phenotype (CIMP) [4].

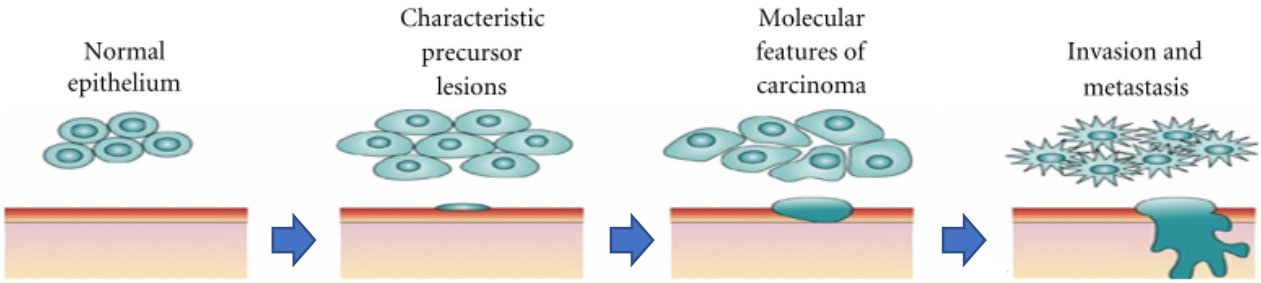

Figure 1. Multistep processes of colorectal cancer formation. *Massimo Pancione et al. Multiple Pathways in Colorectal Cancer Progression*

Genomic stability is strictly controlled to maintain cellular homeostasis [5]. Alteration of the mechanisms that regulate these events promote mutational processes, selection, and clonal expansion of the cancer cells, contributing to tumor progression. The most common type of genomic instability is CIN that characterized the 60% of CRCs. The consequence of CIN is an imbalance in chromosome number (aneuploidy), sub chromosomal genomic amplifications, and a high frequency of loss of heterozygosity (LOH) [6]. CIN pathway starts with the acquisition of mutations in the Adenomatous Polyposis Coli (APC), followed by the activation of oncogene Kirsten Rat Sarcoma (KRAS) (mutated in 30%–50% of CRCs) and the inactivation of the Tumor

suppressor gene, TP53 (reported in 4%–26% of adenomas). Aneuploidy and LOH are the major players in CIN tumors [7]. Microsatellite instability (MSI) is detected in about 15% of all colorectal cancers and is a hypermutable phenotype caused by the loss of DNA mismatch repair activity (MMR). MMR repairs DNA replication errors, inhibits recombination between non-identical DNA sequences, and interferes in responses to DNA damage. Sporadic MSI tumors are commonly described by the hypermethylation and the consequent inactivation of the mismatch repair gene MLH1 [8]. More than 50% of human genes have been found to be regulated by CpG (Cytosine preceding Guanine). CpG islands are regions within the genome in promoter sites that are rich in CpG. In normal cells, several CpG dinucleotides are methylated and, consequently, activated. On the contrary, in cancer cells, the same CpG are unmethylated [9]. This phenomenon is associated with transcriptional inactivation of tumor-suppressor genes in neoplasia. Most of the cancer-specific clones, indeed, were discovered exclusively in a subset of colorectal cancers that exhibits a CpG island methylator phenotype (CIMP) [10]. Many genes with CIMP have important functions in the cell, whereas others have unknown functions [11]. Pathogenetic of CRCs can result from a combination of these three mechanisms that are not mutually exclusive. For example, up to 25% of MSI colorectal cancers can exhibit chromosomal abnormalities [12].

Gastrointestinal tract consists of crypts that comprehend a small number of normal stem cells. Their division is slowly and asymmetrically and generates a population of cells that migrate up the crypt, proliferate, and progressively differentiate. CIN has been described in the transition from normal stem cell to cancer stem cell. It has been proposed that the first mutation in APC occurs in a gastrointestinal stem cell, to generate an $APC^{+/-}$ mutant stem cell. The mutant clone can then colonize the base of the crypt, replacing the non-mutant cells in the stem cell niche [13] . CRCs clinical manifestations depend on the localization of the lesion. Colon lesions occasionally cause haematochezia, bleeding is occult, causing anaemia and fatigue. Rectal lesions cause haematochezia, bleeding, and tenesmus [14] . There is a scientific consensus that the staging of colorectal cancers has a strong correlation with the patients' survival [15] . There are many different ways to staging colorectal cancers. Rectal cancers can be distributed in 4 groups: very early, early, intermediate, and locally advanced [3] . Another tool to describe the stage of CRCs is TNM system. This consist in the classification of tumor through diagnostic tests: Tumor (T) is in the mucosa of colon or of the rectum. Has the tumor spread in lymph Nodes (N)? Has the cancer spread to other part of the body forming Metastases (M)? (*American Joint Committee on Cancer*). The TNM system helps to establish the anatomic extent of the disease. This method allows staging from I-IV, with stage IV being the most severe stage. Stage 0 is used to indicate

carcinoma in situ, which is not considered cancerous but may become cancer in the future, while stage IV is a metastatic cancer [16] . Cuthbert Esquire Dukes (1890–1977) published his seminal paper on the staging of rectal cancer in 1932. His work has stood the test of time because of staging system is an accurate prognostic indicator and a predictor of operative mortality. Dukes' staging is based on resection of the tumor and measures the depth of invasion through the mucosa and bowel wall (*NIH, National Cancer Insitute*). Dukes staging is divided in Dukes' type A, B, C, and D. Dukes stage A bowel cancer; the cancer is only in the inner lining of the bowel. In Dukes stage B, the cancer has invaded the muscle. Dukes stage C is characterized by cancer invasion of the nearby lymph nodes. In Dukes stage D bowel cancer, the cancer has metastasized (*American Society of Clinical Oncology)*. Modified Dukes classification results of histopathological examination and the demographic characteristics of patients and their relation were investigated. Stage A: Tumor limited to mucosa. Stage B1: Tumor limited to the submucosa, no lymph node invasion. Stage B2: Tumors confined to the muscle layer, no lymph node invasion. Stage C1: The tumor did not exceed the bowel wall, lymph node metastasis. Stage C2: Tumor exceeded the intestinal wall and lymph node metastasis. Stage D correspond to the old classification, in which tumor is characterized by distal metastases [17] . The prognosis depends on the time of the diagnosis: in early stage, the treatment is the only surgery [18], but if CRC is diagnosed in advanced state or with metastasis the coupling with chemotherapy is needed [19]. Recurrence, between 5 and 10 years after the initial colon cancer resection with curative intent, occurs in 1 in 17 patients [20].

1.2 Ion channel in tumorigenesis and metastasis

Ion channel receptors are usually multimeric proteins located in the plasma membrane. Each of these proteins arranges itself forming a passageway or pore extending from one side of the membrane to the other. These passageways, or ion channels, can open and close in response to chemical or mechanical signals [21]. All fundamental physiological processes are based on the ability of cells to receive, process, and transmit signals. Signals can be elementary, as small ion movements that create electron potentials across the cell membrane. These channels allow selected ions to flow through the lipid membrane because of changes in the transmembrane potential, ligand binding, or when mechanical forces, temperature, or acidity reach a certain threshold [22] . Ion channels may be classified by the nature of their gating, (Ex. Voltage-gated ion channels open and close in response to membrane potential, Ligand gated; open in response to

specific ligand molecules binding to receptor protein) the species of ions passing through those gates (ex. Chloride channels, Na^+ channels, Ca^{2+} channels, K^+ channels) and the number of gates (pores) and localization of proteins.

Physiological processes depend on the continued flow of ions into and out of cells; Na^+ channels, and in some instances Ca^{2+} channels, are essential for action potential propagation. Molecular analysis of K^+ channels family, revealed their involvement in action potential repolarization, Cl^- channels are involved in volume homeostasis and membrane excitability [23, 24].

Body response to the external stimuli can be linked to the regulation of ion channel activity. Ion channels play a crucial role in various physiological processes including flow of nerve impulses, muscle contraction, cell division and hormone secretion [25]. In organisms with mutations in ion channels, cell proliferation and cell migration can be affected [26].

Ion channels and pumps have a fundamental role in establishment of ideal microenvironment typical of solid tumours and promotion of cancer cells development.

Example of ion channel dependent features could be hypoxia, acidic pH, high levels of lactate, and low levels of glucose [27, 28]. All the cells composing the tumours microenvironment are laden with several types of miss expressed/overexpressed ion channels, which participate in the crosstalk [29].

The role of ion channels and pumps in driving of cancer cells development is has been widely described (Figure 2) [30] .

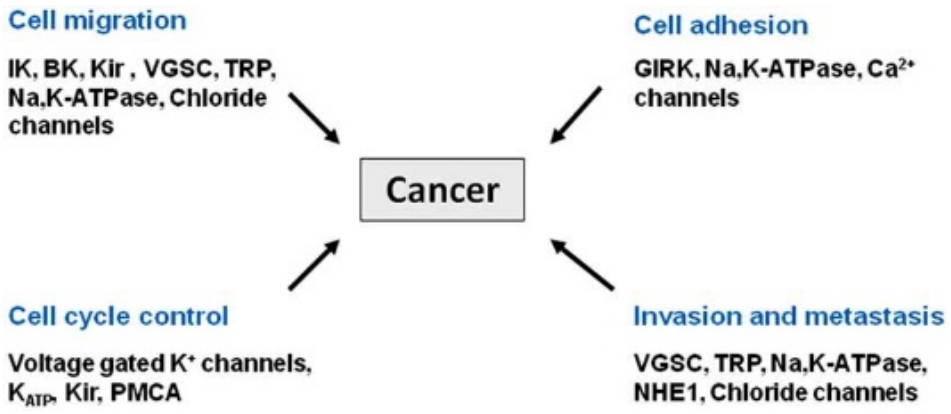

Figure 2. Role of different ion channels and pumps in development of cancer cells. *Cancer as a channelopathy: ion channels and pumps in tumor development and progression [Hospital for Children, Wilmington, DE, USA; 2005]*

They are involved in the acquirement of several hallmarks of cancer as metabolic re-programming [31], limitless proliferative potential [32] , apoptosis resistance [33] , cell migration and invasiveness [34] .

With the flow of time, chloride channels have gained a more prominent importance in carcinogenesis [35] . Chloride channels are expressed ubiquitously both in plasma and on organelles membrane. Here, chloride channels regulate electrical excitability, trans-epithelial fluid transport, ion homeostasis, pH levels, and cell volume regulation, the latter being particularly important for cancer cells migration and infiltration [36] .
The different families of chloride channels retain a heterogeneous regulation of their activity, suggesting a multitask possibility of their participation in the tumorigenesis process [37] .
An emerging class of chloride ionic channels involved in cancer development are the intracellular chloride channels (CLICs). Members of this protein family have been identified in several cancer types such as glioblastoma [38] , and colorectal cancer [39].

1.3 Chloride Intracellular Channel 1

The Chloride Intracellular Channel (CLIC) proteins are highly conserved in vertebrates, with the following six members found in humans: CLIC1 [40] , CLIC2 [41] , CLIC3 [42] , CLIC4 [43] , CLIC5 [44] and CLIC6 [45] . The chloride intracellular channel (CLIC) proteins form a class of intracellular anion channels that do not follow the paradigm of classical ion channel proteins. They can exist as both soluble globular proteins and integral membrane proteins with ion channel function [46] .

CLIC proteins possibly function as tetramers or higher oligomers and have a predicted channel pore in the N-terminus region [47] . Membrane insertion occurs in response to different stimuli from increases of cytoplasmic oxidation to pH changes [48]. Redox changes in neuronal cells causes CLIC1 to migrate to the plasma membrane, whereas a similar change in macrophages leads to nuclear translocation of CLIC4 [49].

Chloride Intracellular Channel protein 1 (CLIC1) is a member of CLIC proteins family. Originally was called Nuclear Chloride Channel 27 (NCC27) since it was identified in cellular nucleus and cytoplasmic organelles of Chinese hamster ovary -K1 cells [50] . It is a protein of 241 amino acids with a molecular weight of 27 KDa, highly conserved among species; indeed mRNA encoding NCC27 is expressed ubiquitous in all tissues [51] .

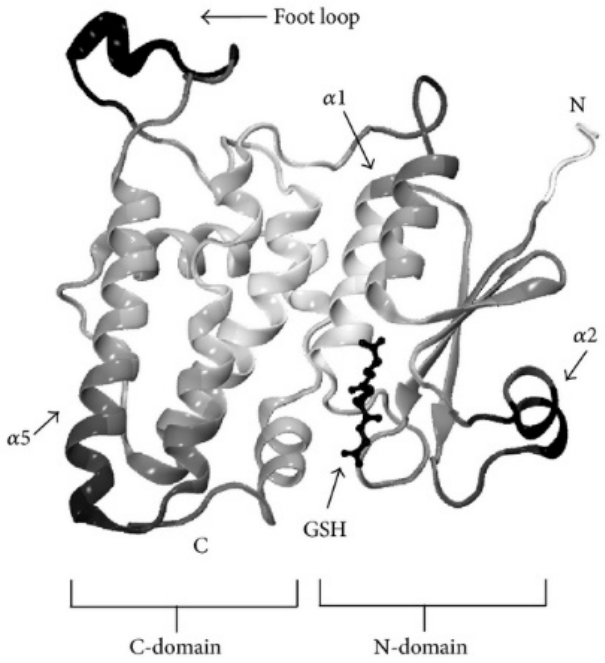

Figure 3. Structure and dynamics of human CLIC1 protein. *Computational Analysis of the Soluble Form of the Intracellular Chloride Ion Channel Protein CLIC1 [BioMed Research International Volume; 2013]*

CLIC1 protein is a non-classical integral membrane protein as a members of the Chloride Intracellular Ion Channel (CLIC) family. CLIC1 is a metamorphic protein: it exists in a cytoplasmic and nucleoplasm soluble form and in a membrane integral form. When it moves from the aqueous phase to the phospholipidic bilayer, CLIC1 acquires ion channel function conducting a chloride current [52] .

The structure of its soluble form does not resemble that of an ion channel. Soluble form of CLIC1 consists of two domains an all α-helical C-domain of 230 aa highly conserved in CLIC family and the N-domain possessing a thioredoxin fold closely resembling glutaredoxin and which is typical of the GST superfamily (Figure 2). CLIC1 contains an intact glutathione-binding site that was shown to covalently bind glutathione via a conserved CLIC cysteine residue, Cys-24. This led to the suggestion that CLIC1 function may be under redox control, possibly via reactive oxygen or nitrogen species. The structure and stoichiometry of the integral membrane form of the CLIC proteins is still unclear. Electrophysiology of purified, soluble (Escherichia coli expressed) recombinant CLIC1 in reconstituted artificial bilayers shows that CLIC1 alone is sufficient for chloride channel formation [53] . The most conserved of these putative transmembrane regions (residues 24–46; CLIC1 numbering) is located within the N-terminal domain and contains Cys-24, which is at the centre of the glutathione-binding site. In the structure

of the monomeric soluble form of CLIC1, this putative N-terminal transmembrane segment forms α- helix (h1) and -strand (s2) within the glutaredoxin-like N-domain [54] .

In 2004, Littler proposed a model to explain the association of CLIC1 with the lipid membrane. This model suggests that in vitro CLIC1 undergoes structural changes upon oxidation, exposing hydrophobic residues that promote the dimerization of the protein, minimizing contact with the aqueous environment of the cytoplasm [53] .

The main structural difference between the monomeric and the dimeric form of CLIC1 is the disappearance of beta-sheet structures. Cysteine 24 and maybe 59 appear to be indispensable for the transition to the dimeric form upon oxidation, probably because the formation of an intermediate disulfide bridge between the two residues stabilizes the dimeric form [55] .

Goodchild and colleagues [56] deepened the role of the oxidation in the process leading to the CLIC1 pore forming transmembrane state. They demonstrated that the dimer is not always required for the membrane insertion. A single CLIC1 monomer can trigger the conformational changes needed for membrane docking. The second step consisted of the membrane insertion of N-terminus and PTM, while C-domain remains in the cytosol. Therefore, the membrane inserted form of CLIC1 shows an external N-domain [50]. NH2-terminal domain of CLIC1 unfolds and crosses the membrane to yield the membrane-inserted form of the molecule [54]. Integral membrane subunits converge to the active CLIC1 ion channel form passing through the CLIC1

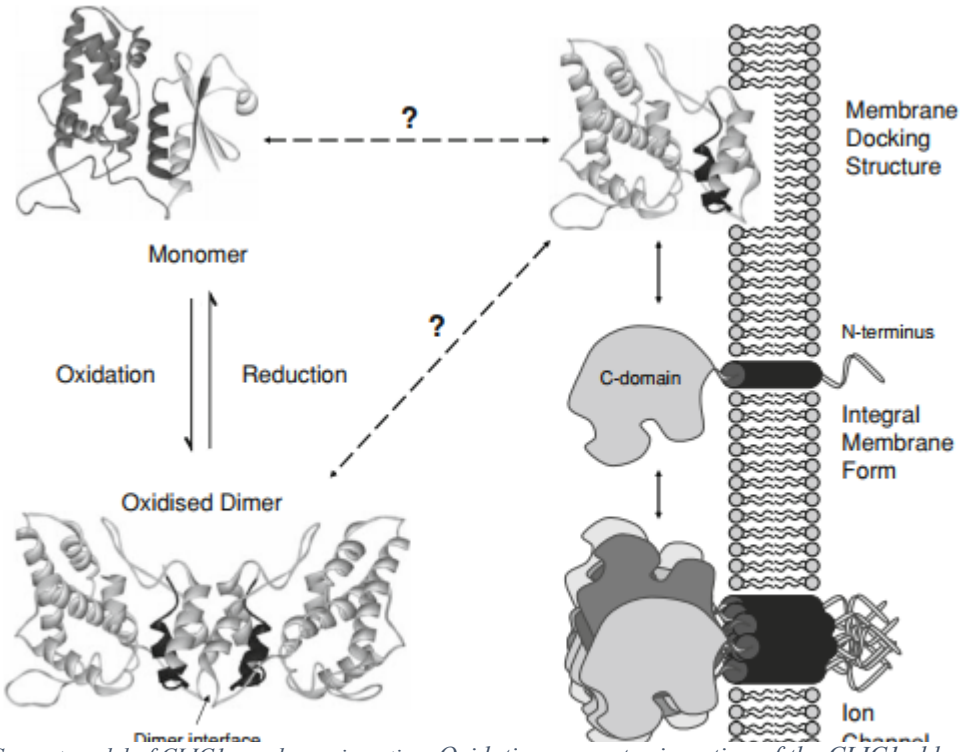

Figure 4: *Current model of CLIC1 membrane insertion. Oxidation promotes insertion of the CLIC1 chloride intracellular channel into the membrane [Biophysics of Structure and Mechanism; May 2009]*

integral membrane intermediate (Figure 4).

Electrophysiological experiments on reconstructed lipid bilayers similar to cell membrane, indicates that CLIC1 ion channel activity is inhibited by Indanyloxyacetic acid 94 (IAA94) and it has been demonstrated that 50 μM IAA94 significantly inhibits the CLIC1-mediated chloride efflux [52].

Electrophysiological experiments performed in CHO-K1 cells transfected with CLIC1 protein revealed biophysical properties of CLIC1 channel activity showing a resting membrane potential of -35 ± 12.4 mV. CLIC1-associated current is sensitive to intracellular changes of chloride concentrations: an increase of intracellular Cl- is consistent with an increase of the single channel conductance [50].

1.4 CLIC1 in solid tumors

CLIC1 expression was found to be correlated with poor prognosis in several solid tumors. According to "The Human Protein Atlas" RNA database, several cancers have shown overexpression of CLIC1 RNA including colorectal cancers, gliomas, breast, lung, ovarian, pancreatic, prostate, and melanoma tumors. Although the role of CLIC1 protein in tumorigenesis is still unclear, diverse studies have investigated the function of CLIC1 in tumor formation and progression. Lu et al. have suggested that CLIC1 is an oncogene in pancreatic cancer. Here, patients in which CLIC1was found overexpressed have demonstrated worse overall survival compared to those with low expression of CLIC1 [92]. CLIC1 expression was correlated to a poor prognosis also in lung [93], ovarian cancer where CLIC1 upregulation confers chemotherapy resistance [94], gallbladder, and gastric cancers [95], where promotes cellular proliferation via MAPK/AKT regulation [95] and helps the formation of tumor-associated fibroblasts [96]. Moreover, CLIC1 protein upregulation correlates with the level of aggressiveness and metastatic potential of colorectal cancer cells [58 59], where it was demonstrated to regulate cell volume and ROS levels. The metastasis of colorectal cancer is one of the most common causes of death. It has been demonstrated that CLIC1, proposed as a novel potential prognostic factor, was significantly up regulated in gastric cancer expressed at the level of the plasma membrane and strongly correlated with lymph node metastasis. The molecular mechanisms of CLIC1 in colon cancer metastasis remain unclear. Functional inhibition of CLIC1 using specific inhibitor IAA94 markedly decreased ROS generation, cell migration, invasion, and phosphorylation of ERK in colon cancer cells [39 ,59]. One of the aspects of cancer is its heterogeneity, it is composed of differentiated cells, representing the major component of the tumor mass, and cancer stem cells (CSCs) [38]. Despite

cancer stem cells constitute a small percentage of tumor cells (0.05-1%), they are the prime sources of tumor recurrence and metastasis as they confer resistance to chemo and radiotherapies [58]. Cancer stem cells are characterized by an aberrant redox system. In particular, it was demonstrated that oxidative stress and gene-environment interactions support the development of a huge variety of solid tumors as colorectal cancer, glioblastoma, breast, prostate, pancreatic and [97]. CLIC1 expression in plasma membrane is strictly dependent on redox homeostasis and pH levels supporting tumorigenesis and development of cancer [62]. Therefore, considering the role of oxidative stress in CSCs, a hypothesis could be that tmCLIC1 protein has an important role in CSCs physiology. In particular, CLIC1 functional activity was assessed in glioblastoma stem cells (GSCs). CLIC1 protein has been found to be chronically expressed in GB CSCs at the plasma membrane level [57]. CLIC1 is overexpressed in glioma tissues where CLIC1 mRNA levels are higher than non-neoplastic cerebral tissues. It has been demonstrated that CLIC1 expression increase is associated with glioma histopathologic grade. Therefore, CLIC1 correlates with human glioma aggressiveness [58]. It is revealed a co-localization between stem/progenitor cell markers (Sox2, Nestin) demonstrating that CLIC1 is enriched in the stem/progenitor cell compartment of the neurosphere. In particular, it is localized on the plasma membrane in GB-derived neurospheres, compared with normal counterparts.

tmCLIC1 protein was demonstrated to have a pivotal role in cell cycle progression and cellular proliferation promoting G1/S cell cycle transition in GSCs. Peretti and colleagues proposed tmCLIC1 to contribute to a feed forward mechanism together with NHE1 proton pump and NADPH oxidase, promoting ROS overproduction [62]. According to these evidence, tmCLIC1 could represent an important target to sensitize CSCs toward chemo and radiotherapies, increasing tumor response to anticancer treatments.

1.5 CLIC1 and ROS regulation

As reported in the previous paragraphs, CLIC1 insertion in plasma membrane is strictly dependent on the oxidation of cell. CLIC1 proteins is formed by 240 aminoacidic sequence belonging to the glutathione S-transferase (GST) fold superfamily. This intracellular structure suggests a role of CLIC1 in redox balance. This GST domain was shown to be the Cys24, and oxidation-dependent insertion is likely to be mediated by the active residue Cys24. Mutations in C24A, indeed, alter the redox sensitivity of the channel and CLIC1 electrophysiological characteristics. High ROS levels provoke a change in the structure of the protein through the

formation of a disulphide bridge between Cys24 and Cys59, considered the essential oxidoreductase residues, promoting membrane docking [53 ,48]. When is expressed as cytosolic monomer, CLIC1 protein binds cytoplasmic GSH. In adverse conditions, the conformational change caused by oxidation promotes the release of GSH, contributing to buffer cytoplasmic oxidation. At the same time, CLIC1 association with an ionic channel guarantees the possibility to disperse any excess of charges that could accumulate during a persistent condition of oxidative stress. [60]. ROS release is supported by the hyperactivation of NADPH oxidase activity, and the mechanism of action by which CLIC1 could help the activation of transitory oxidative phenomenon was investigated by Milton and colleagues. NADPH oxidation causes an extrusion of electrons throughout plasma membrane and the resulting depolarization downregulates the bioenergy of enzymatic activity. CLIC1 conductance during ROS overproduction supports the setting of the resting membrane potential, allowing electrogenic activity of enzymes and ensuring further ROS production. CLIC1 translocation to plasma membrane could be considered a compensative mechanism to support cellular physiological functions in the presence of oxidative stress [61]. CLIC1 activity was reported to be fundamental also in the physiology of glioblastoma stem cells (GSCs) promoting the cells' proliferation enhancing the progression of cell cycle. In particular, as reported by Milton, also in GSCs was reported a feed forward mechanism between NADPH oxidase and tmCLIC1 during G1–S phase transition. Impeding CLIC1-mediated chloride current prevents both intracellular ROS accumulation and pH changes. At the same time, inhibiting NADPH oxidase and NHE1 proton pump results in tmCLIC1 functional activity impairment [62].

1.6 ROS and metastasis

All eukaryotic cells produce Reactive oxygen species (ROS) that have gained importance as regulators of main signaling pathways. ROS are oxygen-containing molecules with high reactivity. They include hydroxyl (HO*) and superoxide (O2*) free radicals and nonradical molecules, as hydrogen peroxide (H_2O_2). H_2O_2 is less reactive but can reach any cellular compartments before its conversion into water and oxygen by peroxiredoxins and glutathione peroxidases. H_2O_2 molecules contribute to redox signaling [63]. The major responsible for ROS production is mitochondria mainly via the electron transport chain, where ~1–2% of O_2 is reduced to form superoxide anions. ROS are also formed in peroxisomes through the β-oxidation

of fatty acids, and in the endoplasmic reticulum for the oxidation of proteins. ROS are also continuously Enzymatic reactions involving cyclooxygenases, NADPH oxidases (NOXs) are involved in ROS production. ROS are also generated after exposure to physical agents (ultraviolet rays and heat) and after chemotherapy and radiotherapy in cancer [64]. In a normal cell, ROS levels are balanced through numerous detoxification processes regulated through antioxidant enzymes. Therefore, ROS homeostasis sustainment contributes to the maintenance of redox balance in healthy cells [65]. Oxidative stress is one of the main leading causes of toxicity which is attributed to the interactions of ROS as well as reactive nitrogen species (RNS) with cellular macromolecules such as DNA, lipid, and proteins, which interfere with the signal transduction pathways such as protein kinases, phosphatases, and transduction mechanisms [66]. In cancer cells the overproduction of ROS is generated from increased metabolic activity, mitochondrial dysfunction, and all the cancer cells features[67]. Mild oxidative stress activates cell signaling mechanisms, such as proliferation, migration, and invasion, but high oxidative stress can induce cell death [68]. Cancer cells are able to rely in a microenvironment in which ROS are overproduced and regulates the acquirement of cancer hallmarks, as abnormal proliferation, cancer migration and invasion. Cell migration is an important process in physiological conditions. It includes a wide array of cellular changes involving alterations in cell structure by, and expression of adhesion molecules. ROS are known to actively participate in all the migration events [69].

ROS are implicated in regulating many integrin-mediated cellular responses, as adhesion, cytoskeleton organization, migration, proliferation, and differentiation. The integrin activation inducts a transient ROS production [70, 71]. Although the mechanisms remain to be defined, there is clear evidence that integrin engagement produces cellular ROS by promoting changes in mitochondrial metabolic function [72, 73, 74]and activation of several oxidases. ROS have a prominent role also in the structure of the cell-cell junction of VE-cadherin [75]. Antioxidant utilization have demonstrated not only that cell-to cell junctions are inhibited, but also that the transcription of pro-angiogenic factor VEGF is impaired [76]. ROS level has been demonstrated to be involved in invasion and metastatic processes in cancer cells. Formation of tumor metastasis requires the disruption of extracellular matrix (ECM) and invasion of the stroma. The activity of the ECM-degrading enzymes is essential for cancer cells to migrate to new sites. These enzymes include the matrix metalloproteinases (MMPs). The invasive ability in cancer cells by increasing MMPs were demonstrated to be dependent by ROS regulation [77, 78, 79]. The ROS levels stimulate the activation of intracellular pathways in relation to tumor invasion including MAPK signaling and regulation of transcription factors upstream of MMPs and uPAs. MMPs activities are

regulated by their endogenous inhibitors, known as the Tissue Inhibitors of MetalloProteinases (TIMPs) [80, 81]. ROS directly control the expression and activity of MMPs also through the blockade of TIMPs [82, 72]. MMPs activity modulated by ROS is reported in several types of cancer cells [83, 84]. ROS are also extremely important in the promotion of Epithelial to Mesenchymal Transition (EMT) [85, 86, 87]. EMT is essential for invasion and metastasis. Taking together, these evidences demonstrate that ROS regulation in cancer cells is essential for several hallmarks of tumorigenesis, in particular for migration and metastasis, that make cancer still uncurable. Recently, the role of ROS and antioxidant is controversial. Piskounova et al. have demonstrated that melanoma metastatic cells have demonstrated a high level of the antioxidant GSH in their cytoplasm [88]. Also other studies have shown that administration of exogenous antioxidants supports cancer cells proliferation and survival signals, allowing metastasis [89]. These new findings open new questions on the role of ROS balance and the antioxidants in tumor progression and clarify the reason why the administration of antioxidants is not effective counteracting tumor development [90].

2. Aims of the thesis

CLIC1 mRNA level was found to be predictive for colorectal cancer prognosis, but its mechanism of action is still unclear. In this scenario, the main aim of the present work is to identify the role of CLIC1 protein in the acquirement of aggressive phenotype of colorectal cancer cells.

We performed several experiments in which was evaluated the expression of CLIC1 protein in different human colorectal cancer cell lines at different level of aggressiveness and its role in tumor proliferation, invasion, and metastasis.

Considering the peculiar metamorphism of CLIC1, which can coexist in cytoplasmic and transmembrane form, we evaluated whether the expression and the functional activity of tmCLIC1as a chloride channel, is proportional to the level of aggressiveness of CRCs.

The specific inhibitor of tmCLIC1, IAA94, demonstrates high toxicity in vivo. In this scenario, our laboratory has designed a monoclonal antibody to specifically recognize 27 aminoacids of the NH_2 domain of tmCLIC1, exposed to extracellular space when the protein is docked in membrane. In the present work, we studied the effect of our antibody, now registered as tmCLIC1omab, on CRCs.

If the inhibitory proprieties of tmCLIC1omab will be confirmed, it can be used as an adjuvant therapy for metastatic colorectal cancer, nowadays still uncurable. In addition, CRCs were engineered to stable silencing CLIC1 protein expression. This was instrumental also to verify whether tmCLIC1 inhibitors are specific, or their effect is due to the presence of off targets.

Moreover, we tried to investigate the mechanism of action of tmCLIC1 in promotion of invasion and metastasis.

Our preliminary experiments have demonstrated that the silencing of CLIC1 modulates the expression of metastatic protein that are directly regulated by ROS levels.

Considering that tmCLIC1 is fundamental in regulation of ROS physiology of cancer cells [62], and the new controversial role of antioxidants in supporting cancer progression [88], we performed several preliminary experiments to elucidate, for the first time, a new mechanism of action in which tmCLIC1 is involved.

3. Materials and methods

3.1 Cell cultures

Human colorectal cancer cell lines were kindly provided by the cell bank of IFOM (Istituto FIRC di Oncologia Molecolare). CCD841 CoN normal colorectal epithelium cell line is cultured in adhesion in Dulbecco's Modified Eagle Medium (DMEM) + 10% of Fetal Bovine Serum (FBS) Penicillin/ Streptomycin (100 U/L) and L- glutamine (2mM) in incubator at 37°C with 5% CO_2. SW480 adenocarcinoma Dukes' type B and SW620 adenocarcinoma Dukes' type D cell lines derived from primary and secondary tumors resected from a single patient, a 50 y/o male. They both growth in adhesion and are cultured in Leibovitz's- L15 supplemented with 10% of FBS, Penicillin/ Streptomycin (100 U/L) and L- glutamine (2mM) in incubator at 37°C without CO_2. COLO201 adenocarcinoma Dukes' type D growth in suspension and are cultured in Roswell Memorial Park Institute (RPMI) 1640 medium supplemented with 10% of FBS Penicillin/ Streptomycin (100 U/L) and L- glutamine (2mM) in incubator at 37°C with 5% CO_2.
Murine colorectal cancer cells CT26 and MC38 were kindly provided by Dr. Carlotta Tacconi from University of Zurich, Switzerland. CT26 growth in adhesion in the same culture medium used for COLO201. MC38 cell lines growth in adhesion and are cultured in the same medium as that as CCD841.
Cells at sub-confluence are routinely passaged using Tryple Express Enzyme (1X) (Thermo Fisher Scientific), centrifuged at 238 rcf for 6 minutes and replated in fresh medium.

3.2 Reagents

tmCLIC1omab (PRIMM s.r.l.) is the monoclonal antibody directed against NH_2 terminal of CLIC1 protein and was selected from a huge number of antibodies derived from four different mice. Polyclonal antibodies were obtained through a 138 days immunization protocol in which mice are immunized against a NH_2-CLIC1 synthetic peptide conjugated to OVA (ovalbumin) (NH_2-EQPQVELFVKAGSDGAKIGNC-COOH) (Glycine 0.1M pH 3, Tris-HCl 1M pH 8). Antibodies specificity was verified by the company through ELISA assay. Hybridoma cells that produced antibodies were sorted in single cells to obtain monoclonal antibodies. A total of 44 different monoclonal antibodies deriving from all of four mice were sent to our laboratory. We then selected among these antibodies the one that shows the best specificity and sensitivity properties.

Indanyloxyacetic acid 94 (IAA94) (Sigma- Aldrich) is used to specific inhibit CLIC1 activity. It was dissolved in absolute ethanol to make a 50 mM stock solution and used at 100 μM working concentration in complete medium.

PD033 isethionate (Sigma-Aldrich); is an inhibitor of cyclin-dependent kinase (CDK) 4 and 6. It was used to synchronize cells in G1 phase of the cell cycle at a concentration of 2.5 μg/ml.

N-Acetylcysteine (NAC) (Sigma-Aldrich) was solved in water to obtained 1M stock solutions. For experiments, NAC was used at 5mM and 0,3 mM.

3.3 Cell RNA extraction and qPCR

This set of experiments were performed thanks to the collaboration with Prof. Tullio Florio's laboratory from University of Genova, Italy. RNA of $3x10^6$ cells were extracted with Monarch® Total RNA Miniprep Kit (New England BioLabs Inc.) according to the protocol given by the company.

Quantitative polymerase chain reaction (qPCR) was used for the quantification of cDNA or genomic DNA and therefore the determination of the expression levels or presence of selected genes. For all performed qPCRs, the PowerUp™ SYBR green master mix (Thermo Fisher Scientific) was used, which contains the Dual-Lock™ Taq DNA polymerase and a green fluorescent dye whose signal is detected for quantification. Primer sequences used for the analysis of CLIC1 gene is listed in table below. Primer solutions, master mix and cDNA samples were pipetted into a 96-well plate according to the pipetting scheme shown in Table 1. All samples were measured in triplicates; and as negative control, water was used instead of cDNA. The plate was closed with a Micro Amp™ optical adhesive film (Applied Byosystem™) and centrifuged for 6 min at 1500 rpm.

Component	Supplier	Volume

PowerUp™ SYBR Green Master Mix	CFX Connect Real-Time PCR System	5 µL/well
Primer F/R (2.5 µM each)	MICROSYNTH	1 µL/well
cDNA		4 µL/well (= 10 ng cDNA/well)
Total reaction volume		10 µL/well

Table 1. Pipetting scheme for qPCR performed in a 96-well plate, using the SYBR Green™ Master Mix, primer solution with 2.5 µM forward primer and 2.5 µM reverse primer and 10 ng of cDNA per well.

The qPCRs for cDNA were run on the *CFX Connect Real-Time PCR System* (BioRad) with the temperature cycles of the "standard program" described in Table below:

	Temperature	Gradient	Time	Cycles
Hold	95 °C	1.6 °C/s	10 min	
PCR	95 °C	1.6 °C/s	10 s	40 x
	60 °C	1.6 °C/s	30 s	
Melt Curve	95 °C	1.6 °C/s	15 s	
	60 °C	1.6 °C/s	1 min	
		0.05 °C/s		

Table 2. Temperature cycles of qPCR experiements

Results were obtained as Ct values, which indicates the number of cycles needed until the fluorescence signal reached a defined threshold. Data were analyzed using the ΔCt method, meaning that the obtained Ct values were normalized over the Ct values of GAPDH (glyceraldehyde 3-phosphate dehydrogenase), a housekeeping gene that should be equally expressed in all cells independent of their treatment. Results are expressed as $2^{-\Delta Ct}$.

Primers used for CLIC1 analysis were the following:

Name	Sequence	Ta	Start..End	Length	GC	Tm
CLIC1_CDS_pcr_forward	ATTACTTAACATCCCCCCTCC			21	47.6	50.5
CLIC1_CDS_pcr_reverse	CCTTTGCCACTTGCTCATAG			20	50.0	51.1
Amplicon	xxx	55.6	425..715	291	52.6	79.1

Figure 4. Forward and Reverse primer sequences for CLIC1 expression level

For qPCR of metastases genes, we performed experiments using RT^2 Profiler PCR Arrays pathway focused gene expression (Qiagen), according to the protocol given by the company.

3.4 Protein extraction and Western blot analysis

Cells were seeded into 35 petri dishes ($4x10^5$ cells/well) and directly lysed with the addition of 60 µL of hot Lysis Buffer (LB) composed by 0.25M Tris-HCl pH 6.8, 4% SDS, 20% Glycerol in water. Then the lysates were scraped off the petri dishes, syringed and boiled for 10 minutes at 95°C to achieve a complete protein denaturation. Samples are centrifuged at 4000 rcf for fifteen minutes and supernatants were collected and stored at -20°C. Protein concentration in the whole cell lysates is evaluated through BCA assay (Thermo Fisher Scientific) following the protocol prearranged by the company. Samples are boiled at 60°C for 30 minutes and the absorbance at 562 nm is read by *Ensight Multimode Plate Reader* (PerkinElmer's).

Protein concentration in whole cell lysates was determinate through normalization with standard BSA (2 µg/ml) straight line.

For each sample, equal amount of protein extracts (30-40 µg) is combined with a certain volume of 4X LDS Sample buffer (Thermo Fisher Scientific) to obtain 1X final concentration and boiled 5 minutes at 95°C. Samples are loaded onto 12% SDS-polyacrilamide electrophoresis gel (PAGE) and run at constant voltage (120 V) for 1-2 h RT in running buffer. Separated proteins were then transferred to a nitrocellulose membrane (Amersham Protran, GE Healtcare) with of 0.45 µm pore size at 100 V constant for 1 h on ice or at 70 V in transfer buffer.

At the end of transfer process, membranes are coloured with Ponceau s solution 0.1 % (w/v) in 5% acetic acid (Sigma-Aldrich) and cut in the correspondence of the molecular weight of interest. Membranes were blocked for 1 h RT to saturate the non-specific antibodies' binding site.

After blocking, membranes were incubated in primary antibodies solutions overnight at 4°C. Membranes are washed three times with washing solution to remove the excess of primary antibodies and incubated 1 h RT with secondary antibody solutions.

After washing, membranes were incubated with SuperSignal® West Femto Maxium Sensitivity Substrate (Thermo Fisher Scientific) 1 minute in the dark. Immunoreactive protein bands were detected using *ChemiDoc Touch*® imaging system (BioRad).

Intensity of the bands corresponds to the protein expression levels. Images were analysed using ImageLab software (BioRad). Values are then normalized to the levels of housekeeping control signal.

Solutions used for western blot assay are the following:

- Separating buffer 4X: 1.5 M Tris-HCl, 0.4% SDS pH 8.8 in H_2O
- Stacking buffer 4X: 0.5 M Tris-HCl, 0.4% SDS pH 6.8 in H_2O
- 12% SDS-polyacrylamide gel: 30% Acrylamide, 10% APS, TEMED, 1X separating/ stacking buffer in H_2O
- Running buffer 10X: 25 mM Tris-HCl, 192 mM glycine, 0.1% SDS in H_2O
- Transfer buffer 10X: 0.02M Tris-HCl, 1% glycine in H_2O
- Blocking solution: 5% w/v BSA in PBS 0.1% Tween® 20
- Staining solution: 3% w/v BSA in PBS 0.1% Tween® 20
- Washing solution: PBS 0.1% Tween® 20
- Secondary antibody solution: anti-mouse and anti-rabbit horseradish peroxidase (HRP)-conjugated (Cell Signalling) diluted 1:10000 in staining solution

Primary Antibodies solutions used are the following:

a. Mouse monoclonal anti-Vinculin (Sigma-Aldrich) diluted 1: 2000 in staining solution
b. Mouse monoclonal anti-CLIC1 (Santa Cruz Biotechnology) diluted 1: 750 in staining solution.
c. Mouse monoclonal antibody anti-Cyclin E (Cell Signalling) diluted 1:1000 in staining solution
d. Rabbit monoclonal antibody anti- MAP38 (Cell Signalling) diluted 1:1000 in staining solution
e. Rabbit monoclonal antibody anti- phospho MAP38 (Cell Signalling) diluted 1:1000 in staining solution
f. Rabbit monoclonal antibody anti- MMP7 (Cell Signalling) diluted 1:1000 in staining solution

3.5 Fluorescence Intensity assay

Fluorescence spectrophotometer analysis was performed to evaluate the total amount of CLIC1 membrane staining in a population of living cells.

1 x 10^6 cells were washed three times and incubated in blocking solution 30 minutes on ice.

Primary antibodies solutions were directly added to samples without removal of blocking solution and incubated for additional 2 h on ice.

After washes, samples were incubated with secondary antibody solution 1 h on ice in the dark.

Samples were washed again for three times and distributed onto a black 96-well plate.
All the washes and staining steps were performed maintaining cells in suspension.
Samples were analysed at *Ensight Multimode Plate Reader* (PerkinElmer's) using appropriate filter to visualize fluorescence intensity emitted by Alexa-Fluor 488 conjugated antibody (Em=488 nm; Ex=350 nm).
Fluorescence intensity values of samples incubated with tmCLIC1omab, are proportional to the amount of CLIC1 transmembrane form and were normalized on the background of single samples obtained with cells stained with only secondary antibody.
Solution used are:

- Washing solution: 1% w/v BSA in PBS, 0.1% sodium azide
- Blocking solution: 5% w/v BSA in PBS, 0.1% sodium azide
- Staining solution: 3% w/v BSA in PBS, 0.1% sodium azide
- Primary antibody solution: tmCLIC1omab diluted 1:140 in staining solution
- Secondary antibody solution: Donkey anti-mouse conjugated to Alexa-Fluor488 (Thermo Fisher Scientific) 1:400 in staining solution

3.6 Patch Clamp experiments

The patch clamp technique allows the measurements of ionic currents passing through single ion channels on plasma membrane. It was developed by Neher ans Sakmann in the late '70 and it has brought great innovation in the fields of physiology and biophysics. In this technique, a small heat-polished glass pipette is pressed against the cell membrane where the ion channels are embedded and form an electrical seal with a resistance of ≈ 1-10 GΩ.
The high resistance of the seal ensures that most of the currents originating in a small patch of membrane flow into the pipette and, from there, into current measurements circuitry.
An electrode (a silver wire coated with AgCl), located inside the glass pipette and connected to circuitry, converts the ionic current into electrical current.
Then we can alter composition and activity of ion channels through utilization of chemical compounds or in electrical way.
There is different way to do patch clamp configuration:

- *Inside out*: Pipette is rapidly withdrawer from the cell-attached configuration without destroying giga seal, leaving a cell-free membrane and allow recordings in known intracellular signals.

- *Whole cell configuration*: After formation of giga-seal, the membrane patch is disrupted providing a direct low resistance access to cell interior, allowing recordings from ion channels of whole cell.
- *Outside-out configuration*: Pipette is gently withdrawed from whole cell configuration without destroying giga-seal, leaving a cell-free membrane patch exposing the bath solution the outer side of lipid bilayer.
- *Perforated patch*: Pipette contains antibiotics (ex: gramicidin) that provide electrical access to cell interior preserving cytoplasm content.

In our experiments, we used perforated configuration.
Patch electrodes (BB150F-8P with filaments, Science Products), with a diameter of 1,5 mm, were pulled from hard borosilicate glass on a Brown-Flaming P-87 puller (Sutter Instrument, Novato, CA) and fire polished to a tip diameter of 1-1,5 μm and an electrical resistance of 3-4 MΩ.
Cells were voltage-clamped using an Axopatch 200B amplifier (Axon Intrument) in perforated patch configuration.
Antibiotic used was Gramicidin in a final concentration in the pipette of 5 μg/mL. Gramicidin forms pores in cell membrane permeable to monovalent cations. This means that internal concentration of chloride is preserved. Clampex 8 was used as interface acquisition program. The voltage protocol consisted of 800 ms pulses from -40 mV to +60 mV (20 mV voltage steps). The holding potential was set according to the resting potential of the single cell (between -40 and -80 mV); a 15 ms prepulse of -40 mV is applied before starting the voltage steps, in this way the different recordings are comparable despite the different holding potential.
CLIC1-mediated chloride current was isolated trough perfusion of specific inhibitor, IAA94 (Indanyloxyacetic acid 94, 100 μM) dissolved in bath solution.
Solution used are the following:

- Bath solution (mM): 125 NaCl, 5.5 KCl, 24 HEPES, 1 $MgCl_2$, 0.5 $CaCl_2$, 5 D-Glucose, 10 NaOH; pH 7.4
- Pipette solution (mM): 135 KCl, 10 Hepes, 10 NaCl; pH 7.4

Analysis was performed using Clampfit 10.2 (Molecular Devices) and OriginPro 9.1. CLIC1-mediated current (IAA94-sensitive current, I_{Iaa94}) was measured by analytical subtraction of residual ionic current after addition of inhibitor from total current (I_{TOT}) of the cell at each membrane potential tested. Current/Voltage relationship were constructed plotting the averaged current density of the least 100 ms of the pulse against the corresponding membrane potential.

Current density (pA/pF) results from the ratio between the ionic current (pA) and cells capacitance (pF). Statistical analyses were performed comparing the slopes (proportional to channel conductance) of the I/V curves of the different groups.

3.7 Growth curves experiments

$2x10^4$ cells were plated in 500 µL of growth medium per well (supplemented with treatment when needed) in a 24-well plate in the absence or presence of IAA94 and tmCLIC1omab. For each experimental condition and time point cells were plated in triplicates. Cells were plated in 24-multiwell and counted at given time points to build up the growth curve. Cells were collected and centrifuged, and the resuspended pellet was diluted 1:1 with Trypan Blue (Life Technologies). Countess II FL automated cell counter (Thermo Fisher Scientific) was used to count them. Data were normalized to their controls.

3.8 3D cultures

$8x10^3$ SW620 and COLO 201 cells were plated in a 20% Matrigel hanging drop to form spheroids in the apex of the drop. After 24h, spheroids were transferred in a rounded 96 well plate coated with 5% of agar in fresh medium in the absence or presence of IAA94 or tmCLIC10mab. Photos were taken every 24h from the initial time point up to 96h to follow spheroids growth. Analysis was performed using ImageJ software for measurements of spheroids' area. Growth rate of the spheroids was obtained through the normalization of area at the different time points on the initial area.

3.9 Cell synchronization

Some of our experiments needed cells synchronization. This passage was useful to obtain a population of cells in the same conditions at the same time. To obtain a high synchronization in G1 we used starvation through serum deprivation for SW620 cell line. Cells are plated in DMEM (Dulbecco Modified Eagle's Medium) + Penicillin (100 U/mL)/ Streptomycin (100 U/mL) and keep in starvation medium from 36 to 60 hours. For COLO201 that are completely insensitive to starvation, was used PD033 CDK4 and 6 inhibitor to synchronize cells in early G1 phase. Cells were treated for 24h to ensure cells' synchronization.

3.10 Cell cycle analysis

Cell cycle analyses were performed through FACS assay by Professor's T. Florio laboratory, University of Genova (Genova, Italy). In our laboratory were performed collection and culture of cells and fixation.

Cells (about $1x10^6$) were synchronized and at the moment of synchronization release were added or not IAA94 and tmCLIC1omab at all the time point chosen. We previously determine different time points from 4h to 26h every two hours. Samples were washed with cold PBS (1X) and fixed with addition of 1mL of cold Ethanol 70%.

Samples are then stored at 4°C and send to Genova for FACS analysis.

3.11 Lentiviral infection

SW480, SW620, COLO20, and MC38 cell lines were infected with shERWOOD UltramiR Lentiviral shRNA according to the protocol from manufacturer (Transomic Technologies). The kit provided four different plasmids, three of them carrying a specific shRNA coding sequence each targeting a particular region of CLIC1 mRNA coding sequence plus one non-targeting shRNA as negative control (SCR). All these plasmids carried ZsGreen fluorophore as a selection marker.

Plasmids were provided as bacterial glycerol stocks and were extracted using ZymoPURE™ II Plasmid Midiprep Kit (Zymo Research). Infected cells were then selected by fluorescent protein expression through sorting at Fluorescence Activated Cell Sorter (FACS) (BD Facs Aria III, BD Bioscience) for each type of plasmid (sh1, sh2, sh3 and SCR). Using FACS analysis to select for cells with highest fluorescent protein expression allows to enrich for the population of cells with the highest frequency of genome editing.

After cell sorting, cells were tested through western blot analysis to evaluate the expression of CLIC1 protein, florescence intensity assay and patch clamp experiments to evaluate the presence of CLIC1 in plasma membrane and its activity as a chloride channel.

3.12 Migration and invasion assays

For migration and invasion assays were used Trans well inserts for 24-well plates (membrane 8.0 μm pores) (Corning). Before plating, cells were starved through serum deprivation for 60 hours. $1x10^4$ cells were plated in the upper reservoir in starvation medium in the absence of presence of IAA94, tmCLIC1omab, or NAC. In the 24-well plate was added complete medium. The chemo attractant gradient resulting from the contact between starvation medium and complete medium let the cell to cross the membrane, but the small pore size block cells in the membrane. After 72h of culture, membranes were stained with DAPI to visualize nuclei. And then included with mowiol on cover glasses. Glasses were conserved in the dark at 4 °C and analyzed under Zeiss Examiner A1 fluorescence microscope with a Zeiss 40X/0.75 NA water immersion objective using DAPI filter to count the number of migrative or invasive nuclei. For invasion assays, Transwell membrane were coated with GelTrex Matrigel (Life Technologies) to mimic the extracellular matrix.

3.13 Zebrafish embryos

Mature adult fishes (approximately 1 year old) were maintained in 3.5 litres tanks (Tecniplast) at 28°C, with water pH between 7.2 and 7.4 and a night/day cycle of 12h. Fishes were fed 3 times per day, and every water parameter was checked and adjusted daily. Fish breeding was performed once a week, by separating males from females during the nighttime and uniting them the following morning, so to have a precise moment when to set the 0 hours post fertilization (hpf). Eggs were then stored in a 28°C incubator for the period needed by the experimental procedure.

Fishes were mate, eggs were collected at 0 hpf and stored at 28°C. At 24 hpf embryos were dechorionated and restored at 28°C until 48 hpf, when the embryos were injected. Cells were harvested until they reached a number between 6 to 8 million, they were centrifuged and resuspended in 50ul of growth medium in a 500ul Eppendorf tube in ice, to avoid cell's aggregation. Microinjections needles were pulled using a Brown-Flaming P-87 puller (Sutter Instrument, Novato, CA), while cells where injected using an Eppendorf Femtojet Microinjector 5247 (Eppendorf). Embryos at 48 hpf have been positioned on a p35 agar plate and anesthetized with Tricaine (164 mg/L): cells were then loaded in the microinjection needle and positioned on the micromanipulator InjectMan NI 2 (Eppendorf). The injection volume was 2 to 4 nl, to have 100 to 200 cells xenografted in every embryo.

Perivitelline space injections: cells were injected in the perivitelline space, in a position where the graft was safe for the major blood vessels in the area. We took the photos right after the injection and stored the embryos in a 48 wells Multiwell in a 32°C incubator with 5% of CO2. Photos were then taken after 48 hours under stereoscope (MZ APO, Leica) with GFP filter to detect the ZSGreen marked cells. At 5 days post-fertilization (3 days after injection) images of the tumors were captured and the relative integrated density – obtained by the product of the fluorescence intensity and the area of the tumoral mass – was calculated as the ratio between the final and the initial tumor integrated density using ImageJ software.

3.14 Murine models

Experiments in murine models were performed in immunodeficient and in immunocompetent mice. Experiments in immunodeficient mice were performed thanks to the collaboration with Dr. Luca Roz from Istituto dei Tumori, Milan.

Immunodeficient mice: NOD/SCID mice were subcutaneously injected in the flank on both side with $1x10^5$ COLO201 cells in SCR and sh1 and sh3 conditions previously mycoplasma free tested. Mice were anesthetized with isoflurane. Tumor mass were measured every 3/4 days with caliber. After 25 days mice were sacrificed, and lungs were obtained and homogenized to visualize metastatic cells.

Immunocompetent mice: 8 weeks old female C57Bl6/J mice were anesthetized with isoflurane and inject with $2x10^5$ MC38 tumor cells (SCR or Sh) in the rectal mucosa with an insulin 300µl syringe. Mice were checked twice a week to verify their health. After 18 days, mice were sacrificed and were obtained rectum, iliac and mesenteric lymph nodes, livers, and lungs. Organs were weighted and lungs and kidneys were homogenized to analyze the eventual presence of metastases.

Organs were homogenized with the following protocol:

All steps on ice (except collagenase digestion at 37°C)

- Mince tissue with scissors, add 4 ml of digestion mix & incubate samples at 37°C for 25 min. on a shaker
- Pass through 70 µm cell strainer into 50 ml Falcon tubes, use plunger of a syringe and 20 ml FACS buffer to wash the filter and drain all cells into the Falcon, centrifuge 6 min. at 500g, discard supernatant by inverting the tube

Basic medium: 2% FCS, 1.2 mM CaCl2, PenStrep (100 units penicillin, 100 µg streptomycin, 100x stock), in un-supplemented DMEM medium (pyruvate free)
Digestion mix 1 for LN: 1 mg/ml Collagenase IV (Gibco) & 40 ug/ml DNase I, in basic medium
Digestion mix 2 for LN and tumor: 3.5 mg/ml Collagenase IV (Gibco) & 40 ug/ml DNase I, in basic medium
Staining protocol: All steps on ice

- Resuspend cell pellets in 100 µl Fc-block (5/62, 1:50 in PBS), transfer to a round-bottom 96-well-plate & incubate 20 min.
- Add 100 µl antibody mix in PBS on top and incubate 20 min. on ice
- Centrifuge 5 min. at 500g and carefully remove supernatant with a pipette
- Resuspend cell pellets in 100 µl FACS buffer to wash, centrifuge 5 min. at 500g, carefully remove supernatant with a pipette & resuspend cell pellet in 100 µl FACS buffer
- Store in the dark at 4 °C until acquisition

Cells were ZsGreen marked, therefore, they can be detected with 488 filter at FACS sorter (BD FACSCanto^{TM}, BD Bioscience).

3.15 Statistical analysis

All data were plotted using GraphPad Prism 7 software (GraphPad Software Inc., San Diego, California), by which all mean values and standard errors have been calculated. Statistical analysis on these data have been performed on the same software. To compare data between two different conditions, unpaired t-test analysis has been used. One-way ANOVA test was used to compare more than two groups within the same experimental condition. Each condition of any experiment was supported by at least 3 independent replicates (n=3). A cutoff value of p value < 0.05 was considered statistically significant.

3.16 Glutathione (GSH) measurements

For detection of GSH levels in human CRCs, we performed experiments used a colorimetric kit GSH+GSSC/GSH assay kit (Abcam plc.) (code: ab239709) following manufacturer instruction.

4. Results

4.1 CLIC1 expression is related to Colorectal cancer cells' aggressiveness

CLIC1 protein was found to be correlated to different pathological states, including cancer. The mechanism of action in tumorigenesis is still unclear, but our previous investigations have revealed that the transmembrane form of CLIC1 (tmCLIC1) is chronically expressed in glioblastoma stem cells, supporting cancer proliferation and development. To evaluate CLIC1 protein role in Colorectal cancer's development, we have chosen different human immortalized Colorectal cancer cell lines (CRCs) at different level of aggressiveness, according to the Dukes' classification. Dukes' staging measures the depth of invasion through the mucosa of colon and bowel wall. Dukes' type A consists in tumor confined to mucosa; type B in which cells invade tissues without the involvement of lymph nodes; type C involves lymph nodes, and type D in which tumors have distal metastases. Cells used were CCD841 (non-cancerous cells, used as a control), SW480 (Dukes' type B), SW620 (Dukes' type C), and COLO201 (Dukes' type D). First, we analyzed the level of expression of CLIC1 mRNA through Real-Time PCR.

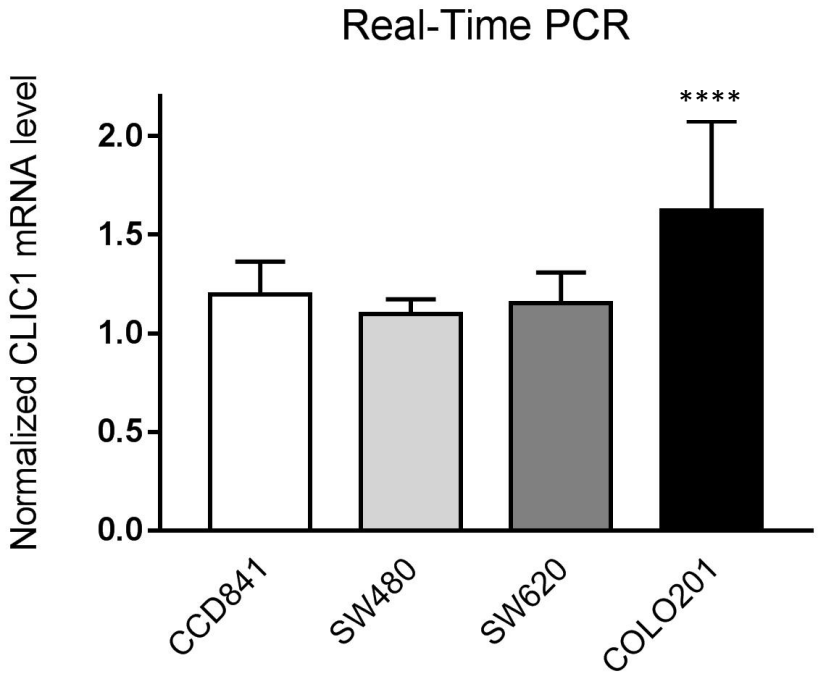

Figure 5. Level of expression of mRNA level of CRCs. Was evaluated the level of mRNA of CLIC1 in cells through Real-Time PCR. The level of CLIC1 mRNA was similar in all cell lines except COLO201 (One-way ANOVA, Tukey's multiple comparison test, ****, p>0.0001)

As depicted in Figure 5, the level of mRNA of CLIC1 is similar in both CCD841, SW480, and SW620, while is significantly higher in COLO201, the most aggressive cell line. Therefore, from a genetically point of view, CLIC1 protein is expressed in all cell lines; in particular, in metastatic cells.

To correlate the expression of CLIC1 mRNA to its presence as protein, we performed a Western blot analysis on all cell lines.

CLIC1 expression was evaluated in relation to the expression of the housekeeping Vinculin. As is visible from the Figure 6, the expression of CLIC1 is proportional to the level of aggressiveness of colorectal cells. CLIC1 expression is significantly higher in CRCs compared to epithelium control, the CCD841. To correlate the expression of the protein to its presence in cells' plasma membrane, different experiments were assessed.

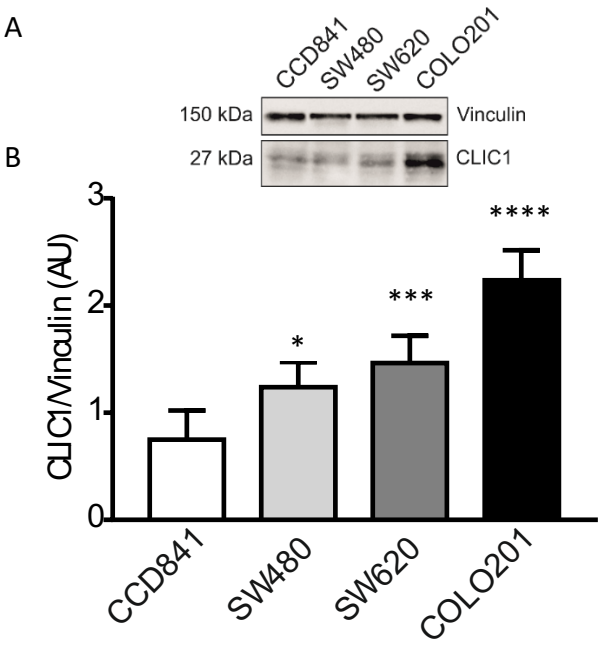

Figure 6. Western blot analysis of CLIC1 protein expression in CRC cells. CLIC1 protein expression significantly increases proportionally with cell lines aggressiveness according to Dukes classification (One-way ANOVA, * CCD841 vs SW480 (1.10 ± 0.006); p<0.05; n=15; *** CCD841 vs SW620 (1.25 ± 0.004), p<0. 005 Tukey's multiple comparisons test, n=13; **** CCD841 vs COLO201 (1.33 ± 0.0035); p< 0.0001, n=15).

First, a fluorescence intensity assay was performed. A living cellular population was decorated with a conjugated monoclonal antibody, designed in our laboratory, to specifically target the NH_2

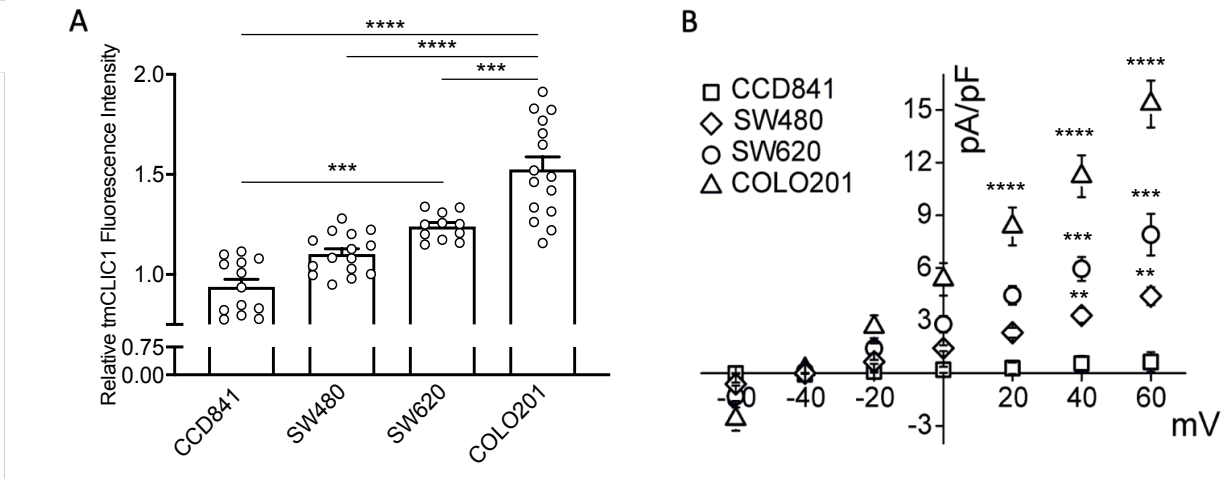

Figure 7. A) Fluorescence Intensity assay on colorectal cancer cells in comparison to non-cancer cells control. The resulting fluorescence is proportional to the expression of tmCLIC1 (One-way ANOVA, CCD841 vs SW620***, p=0. 0003, n=13; **** CCD841 vs COLO201 p< 0.0001, n=15; Tukey's multiple comparison test). COLO201 cells have demonstrated the highest fluorescence intensity signal (One-way ANOVA, **** SW480 vs COLO201, p<0.0001; *** SW620 vs COLO201, p=0.0004, Tukey's multiple comparison test). B) Current density/voltage relationship of colon cancer cell lines. tmCLIC1 current increases concurrently with the invasive potential of tumor (One-way ANOVA, ** CCD841 vs SW480; p<0.01; n=7; *** CCD841 vs SW620, p<0. 005 Tukey's multiple comparisons test, n=6; **** CCD841 vs COLO201; p< 0.0001, n=7).

domain of CLIC1, exposed in the extracellular space when the protein is docked in membrane.

Cells were then analyzed at a fluorimeter and the resulting fluorescence intensity was proportional to the level tmCLIC1. Moreover, to associate the presence of tmCLIC1 to its activity as an ion channel, electrophysiology experiments in perforated patch clamp configuration were performed with the kindly collaboration of Dr. Ivan Verduci.

As depicted in Figure 7A, fluorescence intensity increases proportionally to the invasive potential of cells, confirming that a higher expression of CLIC1 corresponds to an improved presence of tmCLIC1. In addition, from electrophysiology experiments showed in Figure 7B, the tmCLIC1-mediated current obtained after the perfusion of IAA94, the specific inhibitor of tmCLIC1, is significantly higher in CRCs, while is mainly absent in non-cancerous control. tmCLIC1 activity, therefore, is present only in cancerous cells, in particular, in most aggressive cell lines.

4.2 tmCLIC1 inhibition downregulates colorectal cancer cells' proliferation and cell cycle progression

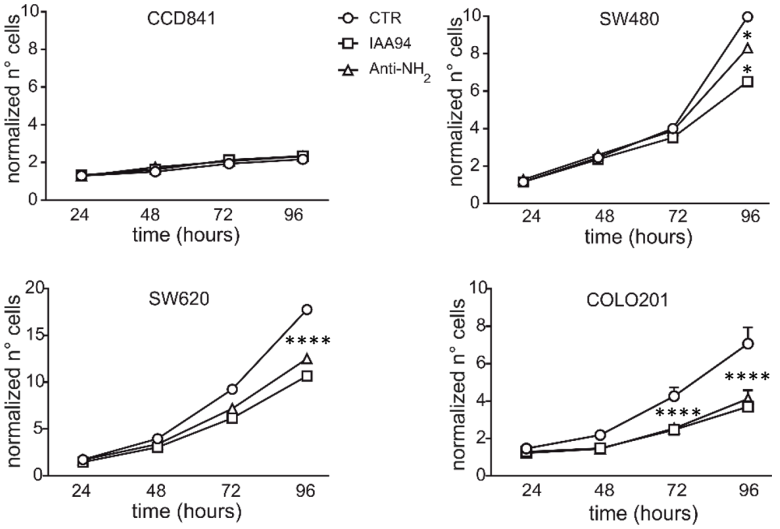

Figure 8. Growth curves of CCD841 (top left), SW480 (top right), SW620 (bottom left), and COLO201 (bottom right) with anti-NH_2 antibody and IAA94 from 24 to 96 hours. Treatments results in a significant decrease of cell proliferation ralated to increasing of CRCs invasive potential. In CCD841 cell proliferation rate is not affected by treatments. SW480 cells show a significantly decrease of cell proliferationafter pharmacological therapies (One-way ANOVA,***CTR vs IAA94, $p<0.005$; ** CTR vs anti-NH_2, $p<0.01$ Tukey's multiple comparison test, n=8). Both SW620 and COLO201 show a significant decrease of cell growth rate (One-way ANOVA, **** CTR vs anti-NH_2, $p<0.0001$; ****CTR vs IAA94, $p<0.0001$, Tukey's multiple comparison test, n=7)

CLIC1 was found to be involved in tumorigenesis and progression of colorectal cancer, but the mechanism of action is still unclear. To demonstrate that the chloride conductance operated by tmCLIC1 ion channel is directly involved in cancer development, we evaluated the proliferation and cell cycle progression of CRCs after the impairment of tmCLIC1 activity using IAA94, and monoclonal antibody mentioned in Figure 7A. Our antibody has demonstrated not only proprieties to target tmCLIC1, but also a good ability to impair its activity. Monoclonal antibody could represent a good alternative to IAA94, considering its high toxicity *in vivo*. To evaluate the role of tmCLIC1 activity in proliferation, we assessed growth curves experiments from 24 to 96 hours in which all cell lines were treated chronically with both IAA94 and monoclonal antibody (Anti-NH_2).

In Figure 8 is visible that in CCD841, neither IAA94 and the antibody have an effect on proliferation of cells, while in Dukes' types B SW480 treatments impair significantly cells' proliferation after 96h. In the most aggressive cell lines, Dukes' type C SW620 and Dukes type D COLO201, both IAA94 and antibody downregulate cellular proliferation significantly after 72 and 48 hours of treatments, respectively. These results demonstrate that the activity of tmCLIC1 is directly involved in tumor progression. To further confirm this result, cells were treated as 3D culture in the absence or presence of both treatments.

These experiments were performed in the most aggressive cell lines, considering that in CCD841 and in SW480 the role of tmCLIC1 is negligible. Spheroids were formed with hanging-drop method and then plated in rounded 96 plate coated with 5% of agar. After the complete formation of spheroids, treatments were added and the area where measured every 24 hours up to 96 hours. The area at each time point was then normalized on the initial spheroids' area.

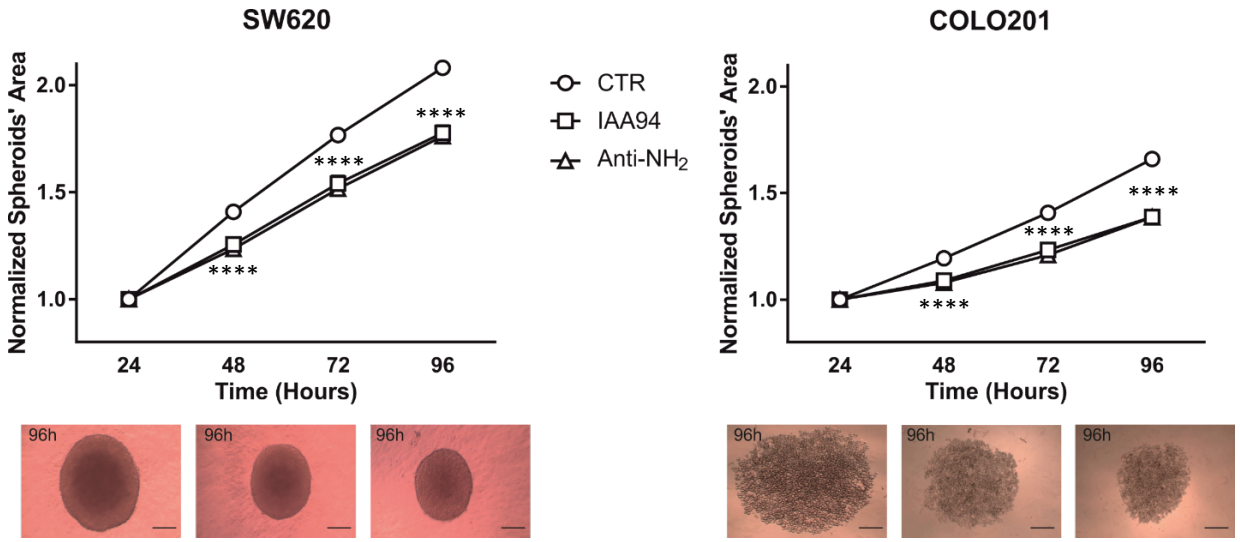

Figure 9. Area's growth rate and representative imagines at 96h of culture of 3D SW620 and COLO201 spheroids treated with IAA93 and anti-NH_2 from 24 to 96 hours. Speroids' area in the presence of CLIC1 inhibitors is significantly smaller compared to the control from 48 hours (One-way ANOVA, **** CTR vs anti-NH_2, $p<0.0001$; **** CTR vs IAA94, $p<0.0001$, n=22. Scale bar: 40uM

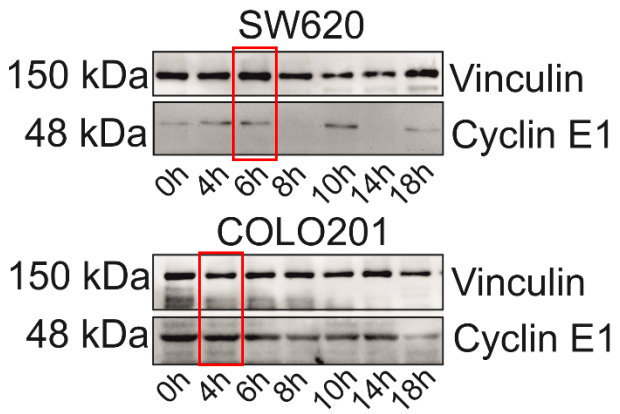

Figure 10. Western blot analysis of cyclin E expression in comparison to housekeeping Vinculin in SW620 (top) and COLO201 (bottom). The red rectangle represents the time point after starvation release in which the peak of cyclin E expression is reached. In SW620 cyclin E peak is reached after 6 hours from starvation release. In COLO201 after 4 hours from starvation release.

after release from cell synchronization. Two differential strategies of synchronization were used in this research: SW620 cells have been subject to 60 hours of serum deprivation, while highly aggressive COLO201 cells, resulting insensitive to conventional starvation, were treated for 72 hours with CDK4/6 inhibitor (see material and methods section). Then, a western blot analysis was performed to quantify the level of expression of cyclin E1, a master cell cycle regulator expressed during the late G1 phase until the end of the S-phase (Figure 10).

In Figure 10 is evident that cyclin E reaches a peak after 6 hours from starvation release in SW620, while its expression is maximum after 4 hours from CDK inhibitor release in COLO201. To evaluate whether tmCLIC1 expression is enriched in G1/S phase transition, we

As is visible from Figure 9, proliferation of spheroids significantly after 48 hours of incubation for both cell lines demonstrating the efficacy of IAA94 and antibody also in more structured complexes.

tmCLIC1 was found to have a role in cell cycle of glioblastoma stem cells (Peretti) promoting the G1/S phase transition. To understand whether this could be a conservative mechanism in cancer cells, we analyzed cell cycle progression of CRCs.

First, we evaluated when G1/S phase occurs

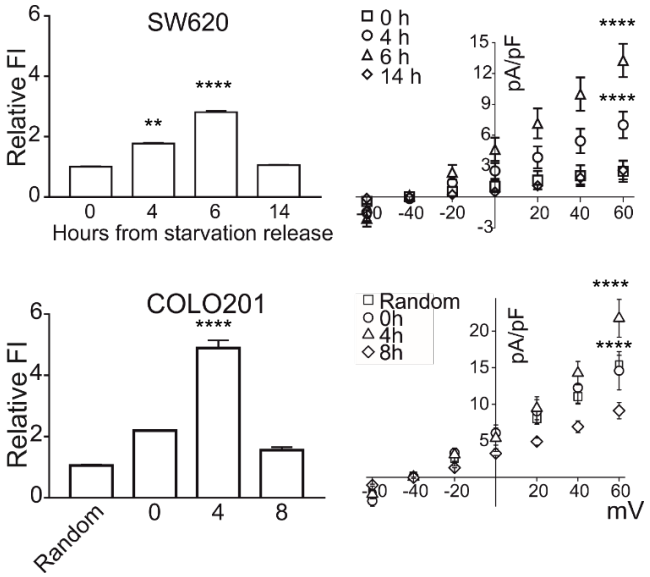

Figure 11. A) Fluorescence intensity assay of SW620 (top) and COLO201 (bottom) at different time points after synchronization release. In SW620, tmCLIC1 fluorescence start to increase after 4h reaching a peak at 7h after synchronization release. tmCLIC1 fluorescence decrease after 14h. (One-way ANOVA; ** 0h vs 4h; **** 0h vs 6h; p<0.005 Tukey's multiple comparisons test, n=15). COLO201 always show an increased level of tmCLIC1 signal compared to the other line. At 4h from CDK inhibitor release, tmCLIC1 signal is significantly increase (One-way ANOVA; **** 0h vs 4h; p<0.001 Tukey's multiple comparisons test, n=15). B) Electrophysiological experiments in perforated patch clamp configuration on synchronised single cells SW620 (top) and COLO201 (bottom). In SW620 CLIC1-mediated current starts to increase after 4h from synchronization release reaching a peak after 6h. CLIC1 mediated current decrease significantly after 14h (One-way ANOVA, **** 0h vs 6h p<0.0001; ** 4h vs 6h p=0.0097; **** 6h vs 14h p<0.0001; Tukey's multiple comparisons test, n=6). COLO201 shows an increase of CLIC1 mediated current in synchronized cells compared to random cells, reaching a peak after 4h from synchronization release (One-way ANOVA, *** Random vs 0h p= 0.0008; **** Random vs 4h p=0.0001; **** 4h vs 8h p=0.0001; Tukey's multiple comparisons test, n=6).

analysed the plasma membrane of CRCs through fluorescence intensity assay and patch clamp experiments at representative time points after synchronization release. Time points were chosen in order to understand whether tmCLIC1 expression is modulated during cell cycle progression. To this purpose, we have chosen 0 hours from starvation release as the starting point. Then, the G1/S transition time point – at 6 hours for SW620 and 4 hours for COLO201 after synchronization release – was analyzed. In addition, we analyzed 14 hours and 8 hours after release, in which cyclin E expression was found to be the lowest.

In Figure 11A is shown the result of Fluorescence intensity assay in both SW620 and COLO201 at the time points mentioned above. In SW620, is visible that after 6 hours from starvation release, the tmCLIC1-depending fluorescence is significantly higher compared to the 0 hours and the 4 hours. At the same time, after 14 hours, when the cells exit from G1/S phase transition, the level of tmCLIC1 fluorescence is superimposable to that of 0 hours. For COLO201, is evident that tmCLIC1 depending fluorescence is maximum after 4 hours from release, fixed as the time point in which G1/S phase transition occurs, while is similar in the other time points. To further confirm this results, we performed electrophysiology experiments as shown in Figure 11B. Patch clamp experiments have been performed at the same time points to that of Fluorescence intensity assay to investigate if the upregulation of tmCLIC1 observed during G1/S phase transition is also associated with an increased chloride channel activity. We show that in both SW620 and COLO201 cells, CLIC1-mediated current is minimal at 0h and reaches the maximum around the timing corresponding to G1/S phase and gradually returns to basal levels (Figure 11B). All together, these evidence suggest that CLIC1 presence is specifically enriched in the plasma membrane during G1/S phase progression. Next, we have evaluated the effect of tmCLIC1 inhibition on the cell cycle progression. To this purpose, the proceeding of the cell cycle of SW620 and COLO201 cells was examined by flow cytometry at different time points after synchronization release. Under serum starvation, SW620 cells were mainly synchronized (more than 80%) in G0 cell cycle phase. Starting between 8 and 10 hours after synchronization release, the number of cells progressed to the S phase gradually increases and reaches a peak at 20 h after release. In the presence of CLIC1 inhibitors the percentage of cells in the G0/G1 compartment increases and, in parallel, the number of cells in S phase decreases at 14, 18 and 22 h after release (Figure 8). Following CDK4/6 inhibition, COLO201 are partially synchronized in advanced G1/S phase. After 4 hours from synchronization release, there is a gradual increase of cells in S and G2 phase. Treatments with IAA94 or anti-NH_2 antibody have led to an accumulation of cells in G0/G1 phase and a parallel reduction in the S and G2 phase fraction, more evident at 14h.

Results obtained confirm that CLIC1 plays a role in cell-cycle progression and its inhibition decreases CRC cells proliferation by G1/S transition delay (Figure 12).

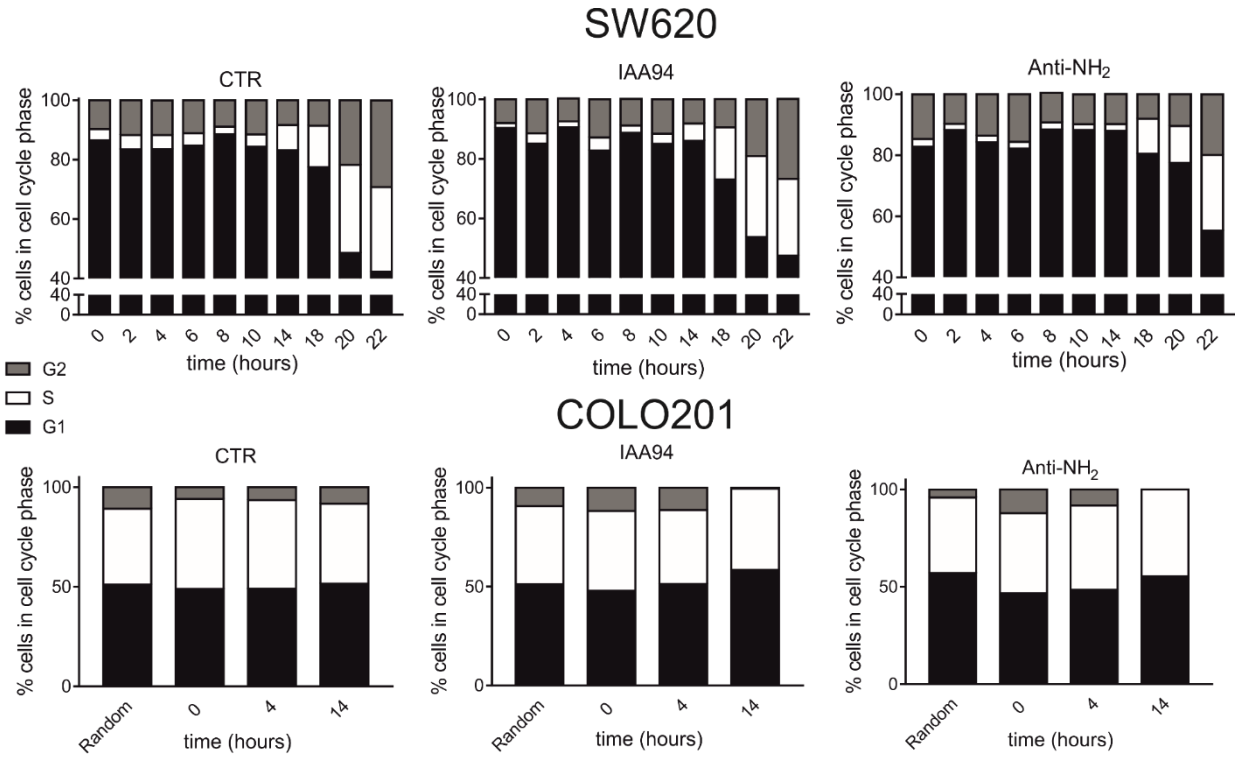

Figure 12. Flow cytometric analysis of cell cycle phases of SW620 (top) and COLO201 (bottom) cells after treatment with or without IAA94 and Anti-NH_2 CLIC1. Inhibitors led to a significant delay of cell cycle progression

4.3 CLIC1 stable downregulation inhibits CRCs 2D and 3D proliferation and delays cell cycle progression

To further demonstrate the specific involvement of CLIC1 protein in promoting CRCs proliferative activity, SW620 and COLO201 cell lines with stable CLIC1 knockdown were established using lentivirus-mediated technology. Vectors carrying two CLIC1-targeting shRNA (sh1 and sh3) sequences, or a scramble control RNA were infected into SW620 and COLO201 cells and the effective downregulation of CLIC1 expression was verified by Western Blotting analysis. In both SW620 and COLO201 cells was

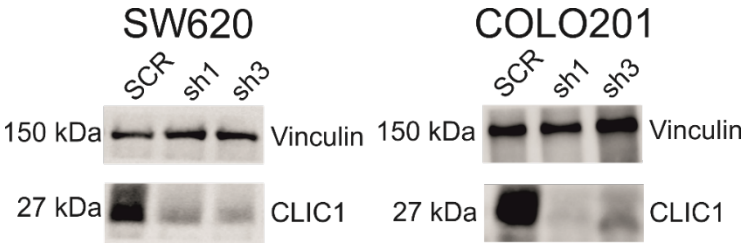

Figure 13. Representative western blot analysis of CLIC1 protein expression in SW620 (top) and COLO201(bottom) clones after lentiviral stable downregulation of the protein compared to the scramble control. In both sh1 and sh3 clones CLIC1 protein expression is mainly absent, while in scramble CLIC1 expression is evident.

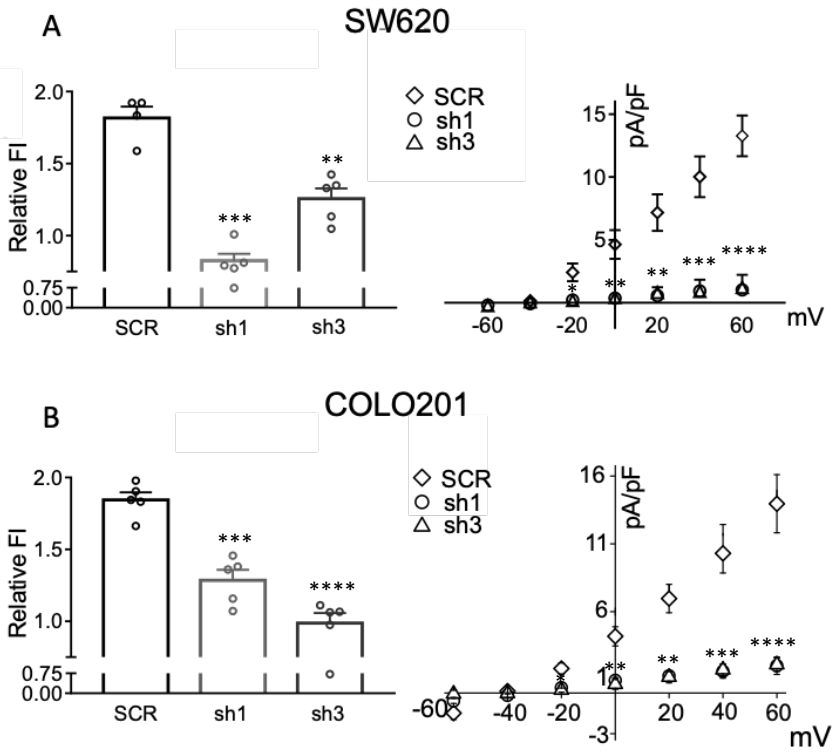

Figure 14. Fluorescent intensity (left) and electrophysiology experiments (right) performed on SW620 (A) and COLO201 (B) knockdown cells. A) SW620 sh1 and sh3 show a significant decrease of tmCLIC1-dependent fluorescence intensity (sh1=1,3 ± 0.125, sh3=1.23 ± 0.072) compared to the scramble control (1.875 ± 0.083) (One-way ANOVA; ** SCR vs sh1, p=0.0020; *** SCR vs sh3, p=0.007; Tukey's multiple comparison test; n=7). Electrophysiology experiments have demonstrated a significative impairment of tmCLIC1-mediated current in all steps analysed (One-way ANOVA; -20 mV, SCR vs sh1 and sh3 *; p= 0.0144; p=0.0282; n=5. 0 mV; SCR vs sh1 **; p=0.0050; SCR vs sh3 *, p=0.0127; n=5. 20 mV SCR vs sh1 and sh3 **, p= 0.0019, p=0.0063, n=5. 40mV SCR vs sh1 ***, p=0.0006; SCR vs sh3 **, p=0.0015, n=5. 60mV SCR vs sh1 **** p<0.0001, SCR vs sh3 ***, p=0.0004, n=5. Tukey's multiple comparison test). B) In COLO201 fluorescent intensity of silenced clones (sh1=1,201 ± 0.202, sh3=1.10 ± 0.12) is significantly higher compared to scramble (2.23 ± 0.094) (One-way ANOVA; *** SCR vs sh1, p=0.00020; **** SCR vs sh3, p=0.0001; Tukey's multiple comparison test; n=7). Electrophysiology experiments (right) have demonstrated a significantly lower tmCLIC1-mediated current in sh1 and sh3 clones compared to SCR control (One-way ANOVA; -20 mV, SCR vs sh1 and sh3 *; p= 0.019; p=0.0291; n=5. 0 mV; SCR vs sh1 **; p=0.0034; SCR vs sh3 *, p=0.015; n=5. 20 mV SCR vs sh1 and sh3 **, p= 0.00134, p=0.0056, n=5. 40mV SCR vs sh1 ***, p=0.00054; SCR vs sh3****, p<0.0001 n=5. 60mV SCR vs sh1 **** p<0.0001, SCR vs sh3 ****, p<0.0001, n=5. Tukey's multiple comparison test).

confirmed a reduction of about 90% of CLIC1 protein expression level following infection with the lentivirus containing the two CLIC1-shRNA constructs, compared with scramble-shRNA vector (Figure 13). We have then performed Fluorescence Intensity experiments to evaluate if the knockdown of the total CLIC1 protein expression is associated also to a decrease in the tmCLIC1 fraction. In both SW620 and COLO201 cells, the amount of specific tmCLIC1 fluorescence staining is significantly reduced in sh1 and sh3 infected cells, compared to scramble cells (Figure 14). Moreover, it has been assessed also whether the downregulation of CLIC1 protein expression is associated with the inhibition of its channel activity through perforated patch clamp electrophysiology experiments. We found that tmCLIC1-mediated current recorded in sh1 and sh3 SW620 cells is significantly decreased compared to the current observed in scramble cells. Similar results were obtained in COLO201 cells (Figure 14). To confirm the role of tmCLIC1 activity on CRCs' proliferation, and to further investigate whether the impairment of

the growth rate seen in Figure 9 is dependent on tmCLIC1 specifically, we evaluated the proliferation rate of silenced cells in 3D cultures.

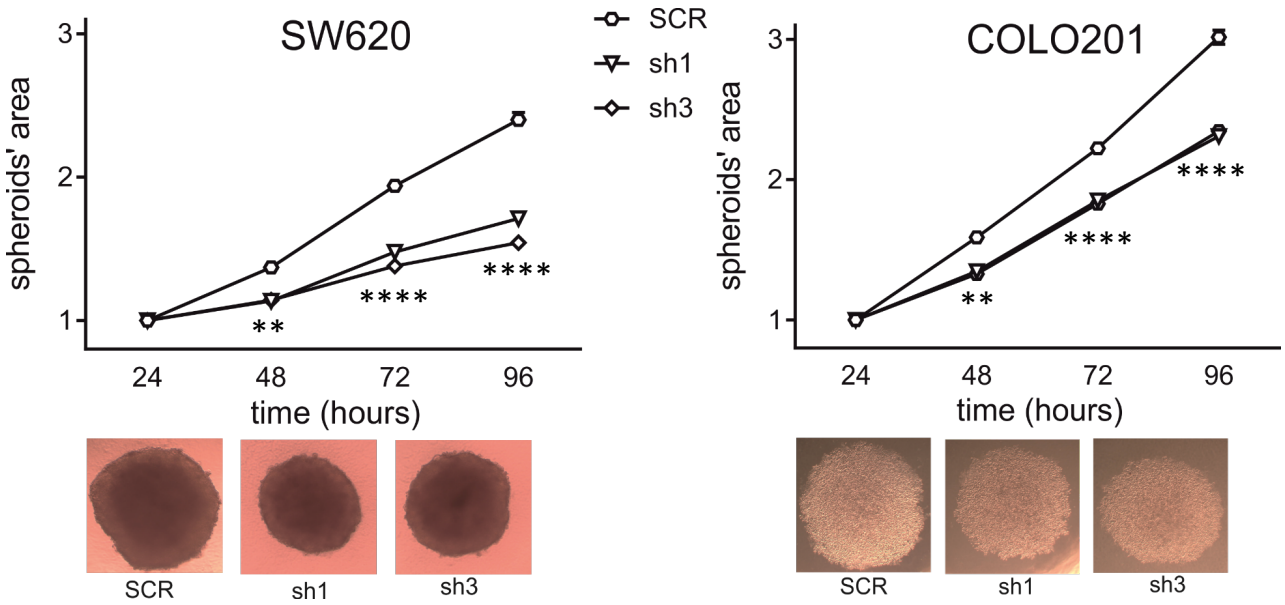

Figure 15. Area's growth rate and representative imagines at 96h of culture of 3D SW620 (left) and COLO201 (right) knockdown spheroids. In SW620, spheroids' area of silenced clones is significantly smaller compared to the control from 72h (One-way ANOVA; *** SCR vs sh1; p= 0.009, n=20; *** SCR vs sh3; p=0.0001, n=20).

The area growth rate of spheroids derived from SW620 and COLO201 infected with CLIC1 sh1 and sh3 is significantly lower compared to SCR spheroids area after just 48h of culture (Figure 15). CLIC1 pharmacological blockage suppresses spheroids growth with an inhibitory effect superimposable to that observed following CLIC1 downregulation. To evaluate whether the delay in cell cycle progression induced by treatment with CLIC1 inhibitors occurs also with stable CLIC1 downregulation a FACS analysis has been performed. Cells were synchronized with the same strategies mentioned in point 4.2, and then the Propidium Iodide fluorescence were evaluated. As represented in Figure 13, SW620 cells infected with CLIC1 sh1 and sh3 show a similar slowing down of cell cycle progression compared to cells after pharmacological treatments, with a reduced percentage of cells in the S phase at 14 and 16 h after release,

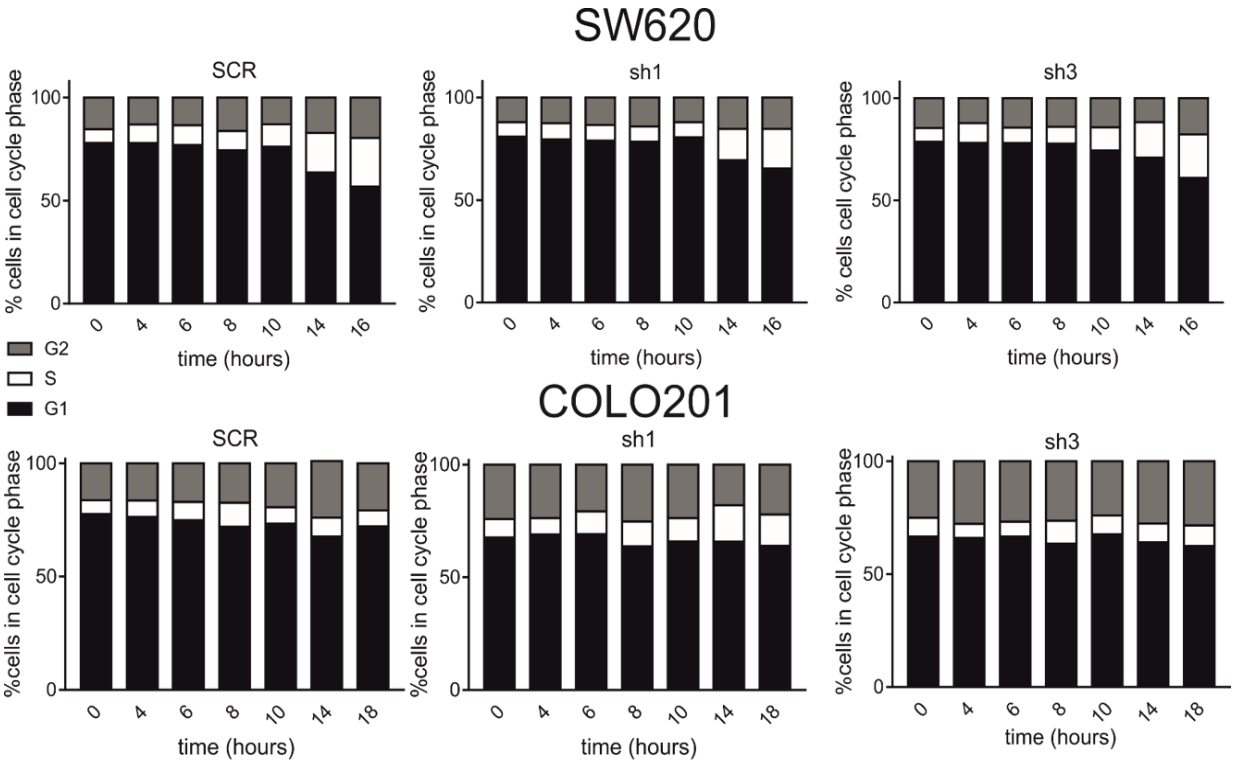

Figure 16. FACS analysis of cell cycle progression SW620 (top) and COLO201 (bottom) SCR, sh1 and sh3 at different time points after synchronization release. In SW620, silenced clones demonstrate an accumulation of cells in G1 phase compared to SCR controls. In COLO201, is visible the increase percentage of cells in G2 phase in silenced clones compared to SCR

compared to SCR control. Similarly, CLIC1-silenced COLO201 cells showed a significant increase in the number of cells in G1 phase and a marked decrease in S and G2 phases. The obtained results further confirm the role of CLIC1 activity in cell-cycle progression, and that the effect of pharmacological inhibitors used in the experiments in point 4.2 is strictly dependent by their action on tmCLIC1 activity.

4.4 tmCLIC1 impairment affects migration and invasion *in vitro*

The overexpression of tmCLIC1 in the most aggressive cell lines of colorectal cancer, opens a question on the function of tmCLIC1 activity on migration and invasion potential of CRCs, that makes colorectal cancer still uncurable. We performed a Trans well assays to understand whether CLIC1 impairment could affect the migration and invasion potential of both SW620 and COLO201. Cells were plated after 60 hours of serum deprivation on a porous membrane, permeable only to growth factor, in contact to complete medium. The resulting chemo-attractant gradient will lead the migrative cells to cross the membranes that were then stained with DAPI to visualize the nuclei. We evaluated the behavior of WT cells after treatment with both IAA94

and monoclonal antibody and of knockdown cells. After 72h of culture, as is depicted in Figure 17, in both treated cells and CLIC1 knockdown cells, the migration potential is significantly impaired compared to controls. For invasion assays, we coated with Matrigel the porous membrane to mimic the extracellular matrix that cells must disrupt to invade tissues and mucosa.

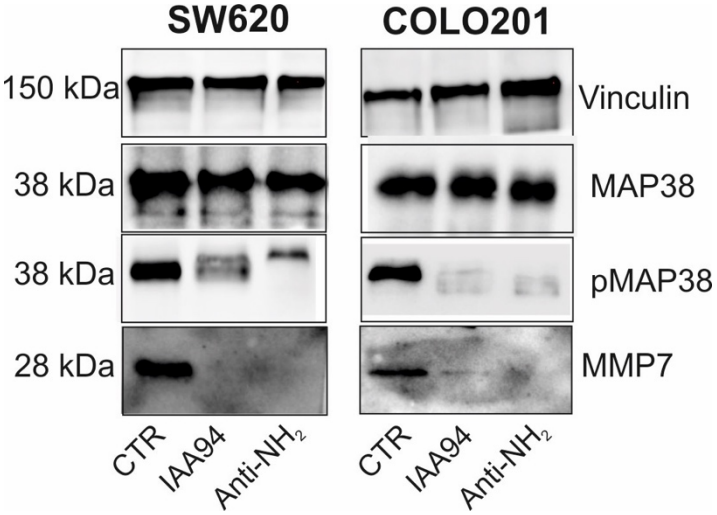

Figure 17. Western blot analysis of MAP38 in its total and activated phosphorylated form and Metalloproteinase 7 in SW620 (left) and COLO201 (right) after 72h of treatment with IAA94 and monoclonal antibody. In SW620 is visible that the expression of pMAP38 is downregulated in the presence of both treatments, and the expression of MMP7 is mainly abolished in the presence of IAA94 and antibody. In COLO201 the results are superimposable to what was seen in SW620

Also in this case, after 72h of culture, is visible that the number of invasive nuclei is significantly lower in treated and silenced cells compared to controls, demonstrating that CLIC1 impairment results in the block of invasive and migration potential (Figure 18). Considering that migration and invasion potential are regulated by a huge number of protein family, we investigated the effect of tmCLIC1 inhibition of the expression of two of the most representative proteins involved in invasion and migration of colorectal cancer cells. We evaluated the expression of Mitogen-Activated Protein Kinase 38 (MAP38) in its total and phosphorylated form (pMAP38) that was found to be extremely important for migration and overexpressed in our CRC lines, and the Metalloproteinase 7 (MMP7), found to

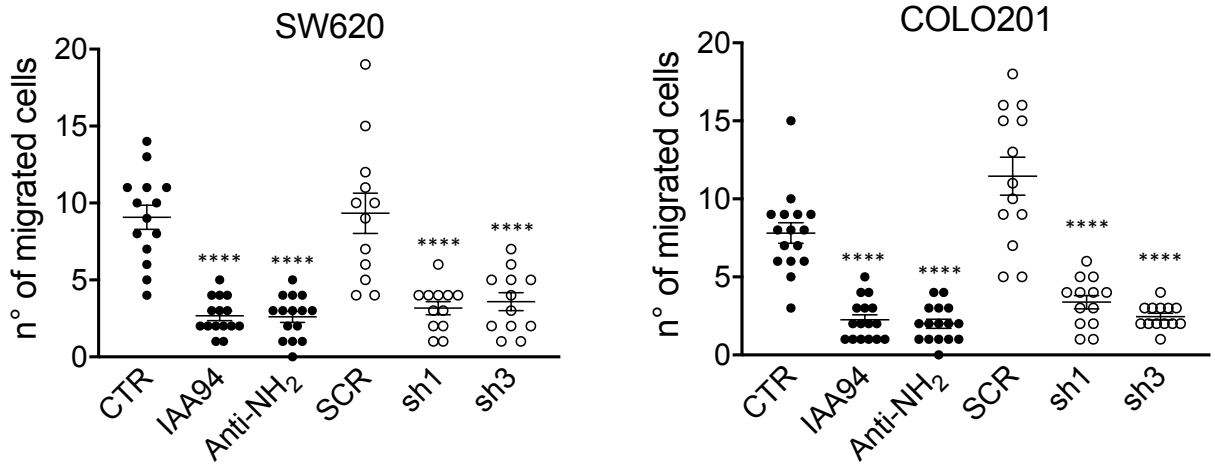

Figure 18. Transwell Migration assay. SW620 (left) and COLO201 (right) of WT cells treated with IAA94 and Anti-NH_2(black dots), and knockdown cells (clear dots). SW620 cells clearly demonstrate a significant lower number of invasive nuclei in presence of both IAA94 and antibody compared to control (One-way ANOVA, CTR vs IAA94 ****, $p<0.0001$; CTR vs Anti-NH_2 ****, $p<0.0001$, Tukey's multiple comparison test n=19), and of silenced cells compared to SCR control (One-way ANOVA, SCR vs sh1 ****, $p<0.0001$; SCR vs sh3 ****, $p<0.0001$, Tukey's multiple comparison test n=13). COLO201 cells show the same behavior seen for SW620 (One-way ANOVA, CTR vs IAA94 ****, $p<0.0001$; CTR vs Anti-NH_2 ****, $p<0.0001$, Tukey's multiple comparison test n=16; SCR vs sh1 ****, $p<0.0001$; SCR vs sh3 ****, $p<0.0001$, Tukey's multiple comparison test n=14).

be a key regulator of invasive mechanisms and overexpressed in both SW620 and COLO201. As shown in Figure 19, in both SW620 and COLO201 the expression of the activated form of MAP38 (pMAP38) is significantly impaired compared to control. At the same time, also MMP7 expression is mainly abolished in the presence of tmCLIC1 inhibitors demonstrating that the alteration of tmCLIC1 activity has a consequence on the expression of the most important proteins involved in migration and invasion potential.

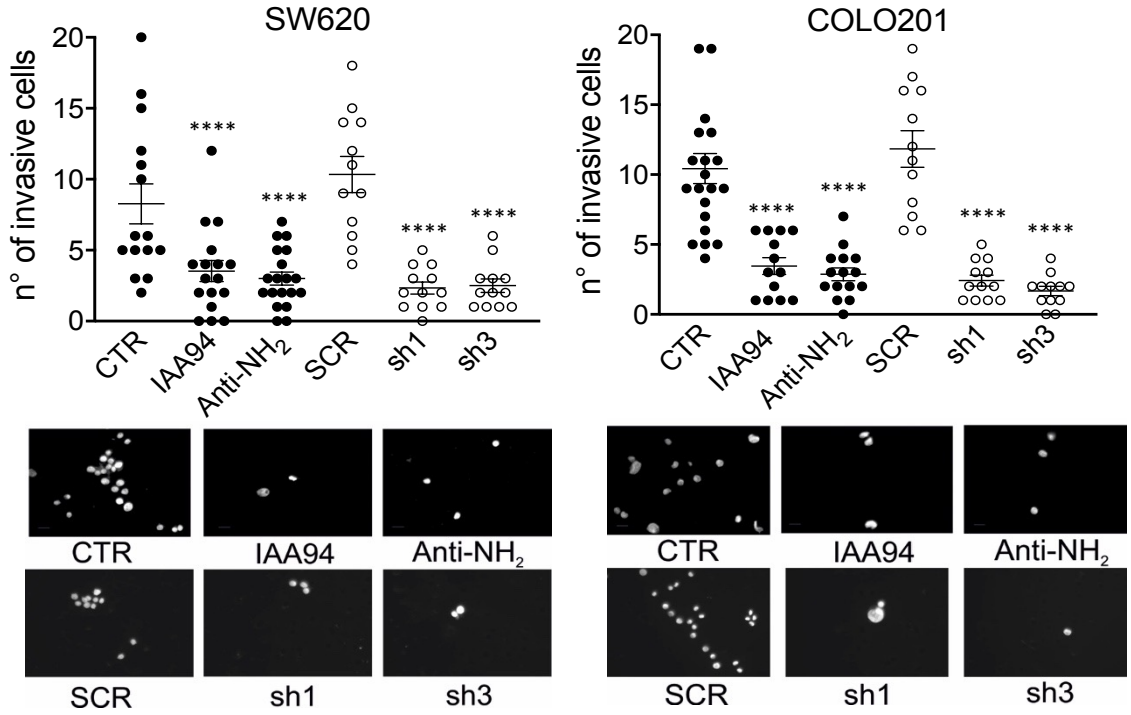

Figure 19. Transwell assay for evaluation of invasion potential of SW620 (left) and COLO201 (right) of WT cells treated with IAA94 and Anti-NH_2(black dots), and knockdown cells (clear dots). SW620 cells clearly demonstrate a significant lower number of migrative nuclei in presence of both IAA94 and antibody compared to control (One-way ANOVA, CTR vs IAA94 ****, $p<0.0001$; CTR vs Anti-NH_2 ****, $p<0.0001$, Tukey's multiple comparison test n=14), and of silenced cells compared to SCR control (One-way ANOVA, SCR vs sh1 ****, $p<0.0001$; SCR vs sh3 ****, $p<0.0001$, Tukey's multiple comparison test n=12). COLO201 cells show the same behavior seen for SW620 (One-way ANOVA, CTR vs IAA94 ****, $p<0.0001$; CTR vs Anti-NH_2 ****, $p<0.0001$, Tukey's multiple comparison test n=16; SCR vs sh1 ****, $p<0.0001$; SCR vs sh3 ****, $p<0.0001$, Tukey's multiple comparison test n=13). On the bottom is reported a representative picture of the membranes after 72h of treatments. Scale bar: 20uM

4.5 Knockdown of CLIC1 inhibit tumor proliferation and invasion in zebrafish embryos

4.6 To investigate whether the inhibition of tumorigenesis could depend on tmCLIC1 impairment in more complex system, we investigated the proliferation and the formation of metastasis in zebrafish embryos. Zebrafish embryos are a very good model to study tumorigenesis and cancer development. We injected SCR and silenced SW620, ZsGreen marked, in perivitelline space of embryos after 72h post fertilization. This site of injection gives the possibility to the tumor to create a new network of vascularization and to growth in the best way [91]. After 72h post injection was evaluated the density of the tumor and compared to the initial mass (see Material and Methods section).

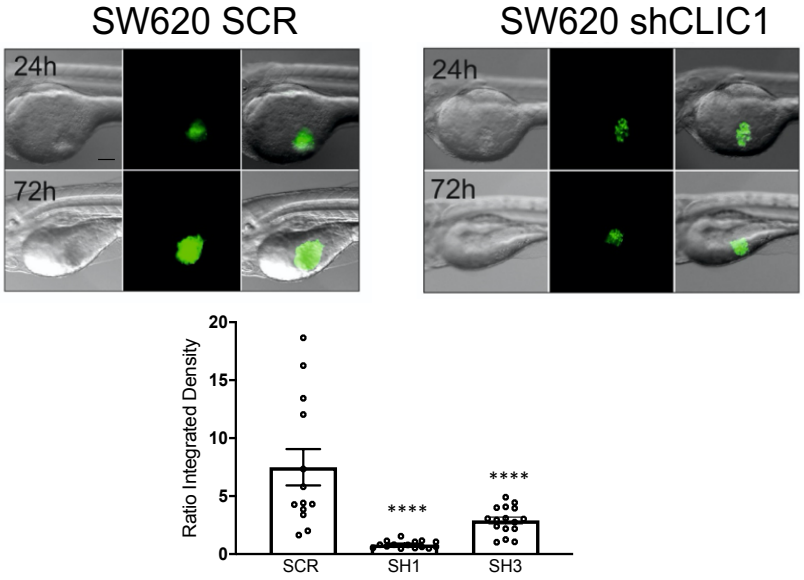

Figure 21. (top) Representative picture of zebrafish embryos after 24h and 72h post injection of SCR (left) and shCLIC1 (right) cells. Scale bare: 200uM. (bottom)Ratio integrated density obtained by the normalization of tumor masses after 72h on masses measured after 24h post injection. Silenced tumors have demonstrated a ratio integrated density significantly lower compared to SCR tumors. (One-way ANOVA, SCR vs sh1 ****, p<0.0001; SCR vs sh3 ****, p<0.0001; Tukey's multiple comparison test, n=16

As demonstrated in Figure 20, the tumor masses formed by silenced cells is significantly lower

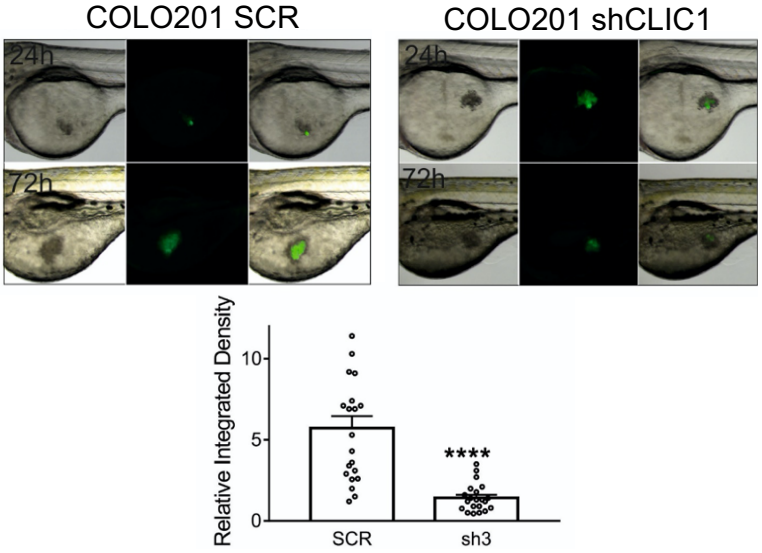

Figure 20. (top) Representative picture of zebrafish embryos after 24h and 72h post injection of SCR (left) and shCLIC1 (right) cells. Scale bare: 200uM. (bottom)Ratio integrated density obtained by the normalization of tumor masses after 72h on masses measured after 24h post injection. Silenced tumors have demonstrated a ratio integrated density significantly lower compared to SCR tumors. (One-way ANOVA; SCR vs sh3 ****, p<0.0001; Tukey's multiple comparison test, n=24)

compared to the tumor masses of SCR control. The same experiment was performed also injecting COLO201 in SCR and silenced conditions.

COLO201 show a significant downregulation of tumor proliferation in the absence of CLIC1 protein results in zebrafish embryos as well (Figure 21). Considering that tumors in perivitelline space are vascularized, we evaluated also whether tumors were able to form distal metastases other site of the embryos. After 72h post injection, we analyzed the yolk sac, the brain, the eyes, the heart, and the tail of the embryos, known to be site of metastases. Here, the percentage of the tumor that were able to form metastases in one of the mentioned sites on the total tumors injected was calculated.

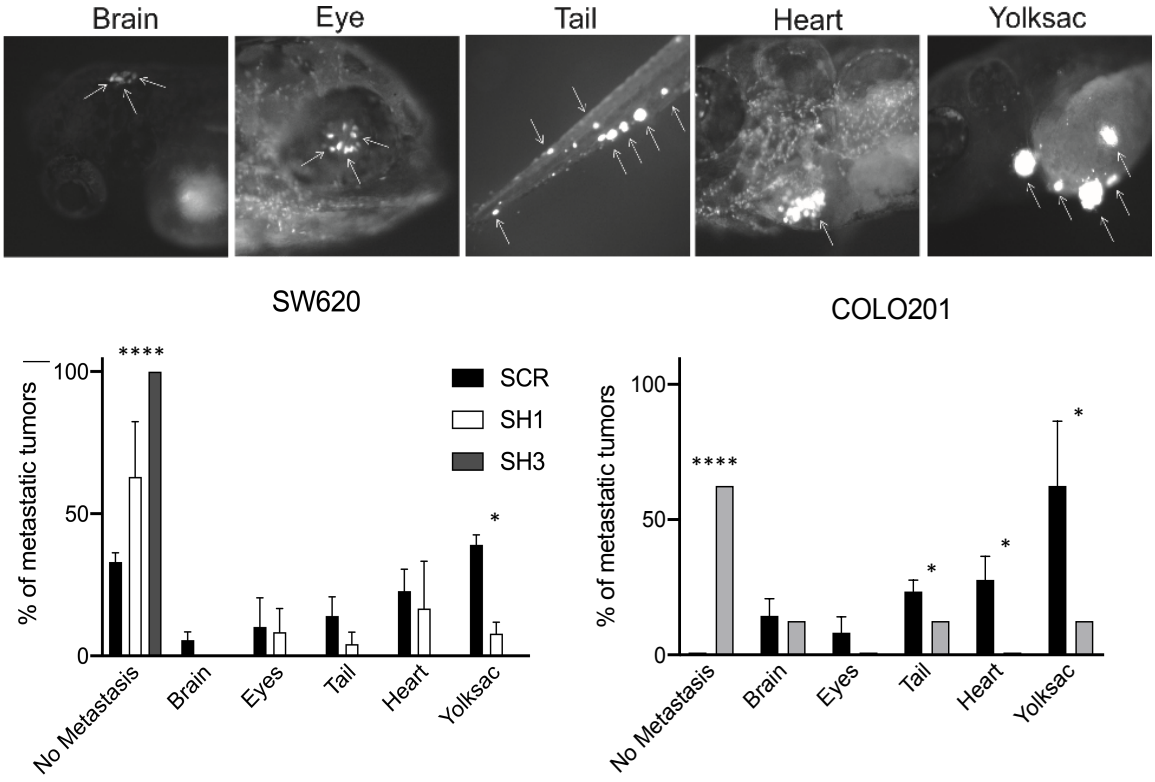

Figure 22. (top) Representative picture of metastases in distal site from primary tumors. With the white arrows are indicated the metastases in brain, eye, tail, heart, and yolk sac. Scale bar: 200uM. (bottom) Percentage of tumors that have formed or not metastases in distal site. In SW620 (left) SCR tumors (black column) have formed significantly more metastases compared to sh1 tumor (white column) and sh3 tumors (grey column) (One-way ANOVA, No metastasis, SCR vs sh1 and sh3 ****, $p<0.0001$ Tukey's multiple comparison test n=; Yolksac SCR vs sh1 *, $p=0.018$, student t test unpaired nonparametric. In COLO201 (right) SCR tumors (black column) have formed always metastasis compared to sh3 tumors (grey column) that have not formed metastases in more than 60% of the cases (Student t test, unpaired non paramentric comparison; No metastasis SCR vs sh3 ****, $p<0.0001$; Yolksac *, $p=0.0495$; Heart *, $p=0.0495$; Tail *, $p=0.0253$)

As depicted in Figure 22, in SW620 SCR tumors have formed metastasis in the 40% of the cases in yolksac, in the 33% of the cases in heart, 20% in tail and brain, and less than 10% forms metastasis in brain. Moreover, less than 40% of tumors have not formed any metastases. More than 60% of sh1 tumors were not able to form any metastases. Less than 20% have formed metastases in heart, and less than 10% of tumors have formed metastases in yolksac, and in eyes while no metastases were found in brain. At the same time, all the sh3 tumors injected was not

able to form any metastases. In COLO201, all SCR tumors were able to form metastases in distal sites. In particular, more than 65% of tumors formed metastases in the yolksac, while more than 30% of the tumors have generated metastasis in the tails and in the hearts. At least, more than 10% of SCR tumors have metastases in brains and in eyes. Silenced COLO201 tumors where not able to generate metastases in more than 60% of the cases, while less than 20% of tumors have formed metastases in yolksac, tails and brains. These results were fundamental to better define the pivotal role of CLIC1 activity in tumorigenesis, and in tumor progression *in vivo*, confirming the results obtained *in vitro*. This evidence could be considered a starting point to study more in deep a treatment against tmCLIC1 activity in metastatic colorectal cancer cells.

4.7 CLIC1 impairment affects tumor progression and metastases formation in immunodeficient mice

Tumor development and progression was evaluated in immunodeficient mice. 1 x 10^5 mycoplasma free cells were injected subcutaneously in the flank of immunodeficient mice. Tumor volume was measured every 3-4 days with a caliber up to 27 days. After 27 days post injection, as shown in Figure 23, sh3 tumor volume is significantly lower compared to SCR controls, while sh1 tumors have a growth rate superimposable to that of SCR tumors. After the sacrifice, mice lungs were analyzed to evaluate metastases formation. After the homogenizations of the tissue, cells were hybridized with an anti-human antibody and then examined through FACS analysis in order to identify the percentage of human cells moved from tumor primary site.

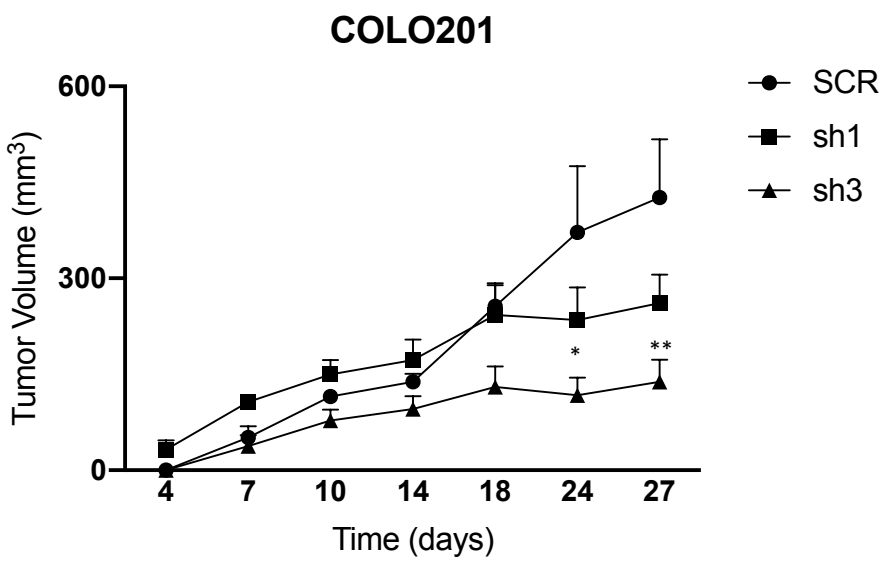

Figure 23. Tumor volume of COLO201 injected subcutaneously in immunodeficient mice. SCR (black dots) sh1 (black square), and sh3 (black triangle) tumors were measured every 3-4 days post injection with a caliber. Sh3 tumor volume is significantly lower compared to SCR tumors (One-way ANOVA, 24 days: SCR vs sh3 *, p=0.0213, SCR vs sh1 ns Holm-Sidak's multiple comparison test. 27 days: SCR vs sh3 **, p=0.0049, Bonferroni's multiple comparison test, n=6)

As depicted in Figure 24, the percentage of Disseminating Tumor Cells (DTCs) in mice lungs was significantly lower (approximately 0,9%) in sh3 tumors compared to SCR tumors (approximately 2,5%). Although sh1 tumors have demonstrated a growth rate superimposable to that of SCR tumors, the percentage of DTCs found in mice lungs was significantly lower (approximately 1,1%) compared to controls. This could be explained by the fact that metastases processes and proliferation pathways are regulated by distinct pathways.

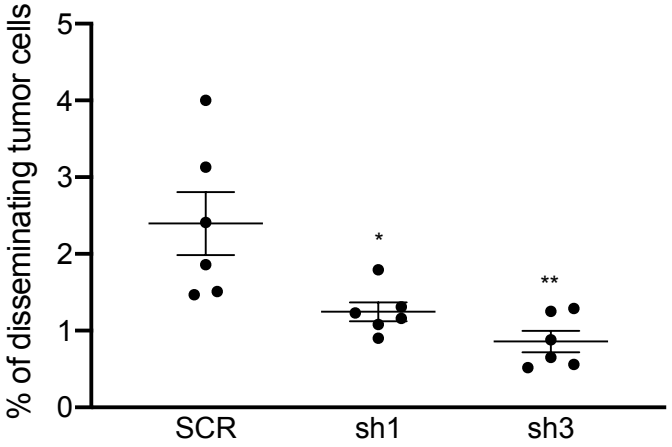

Figure 24. Percentage of disseminating tumor cells (DTCs) in mice lungs of COLO201 SCR, sh1 and sh3. Both sh1 and sh3 have demonstrated a lower percentage of DTCs compared to SCR cells (One-way ANOVA, SCR vs sh1 *, p=0.0129; SCR vs sh3 **, p=0.0015; Dunnett's multiple comparison test, n=6)

Considering that subcutaneously injection is not the best way to evaluate tumor development and progression, we planned to perform orthotopically injection in immunocompetent mice using murine colorectal cancer cells.

4.8 Murine colorectal cancer cells have the same phenotype of human colorectal cancer cells

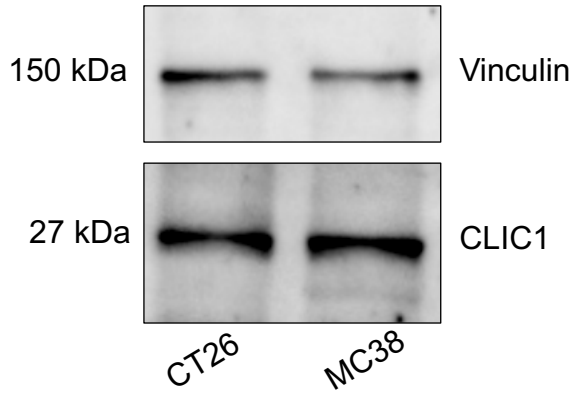

Figure 25. Western blot analysis on murine immortalized colorectal cancer cells CT26 (left), and MC38 (right). At 150kDa is visible the housekeeping Vinculin. CLIC1 signal correspond to 27kDa. Both cell lines demonstrate the same level of expression of CLIC1 protein.

In vivo experiments have been performed in human colorectal cancer cells that have specific phenotype. They have demonstrated the overexpression of CLIC1 protein, and a high tmCLIC1 localization and activity. Therefore, two murine immortalized colorectal cancer cells, CT26 and MC38, were tested for CLIC1 expression, tmCLIC1 activity, tumor proliferation, and invasion. First, a Western blot analysis was assessed. In both CT26 and MC38 cell lines the level of

expression of CLIC1 protein is similar to that of SW620 and COLO201, as represented in Figure 6 (Figure 25). To further correlate the expression of CLIC1 protein to its localization in plasma membrane, a Fluorescence Intensity assay was performed. Here, the tmCLIC1-dependent fluorescence of CT26 and MC38 was compared to the fluorescence measured in human colorectal cells, including non-cancerous-line CCD841 and Dukes' type B SW480. As depicted in Figure 26, grey column represents the signal derived from CT26 and MC38. The level of fluorescence in CT26 cell line is superimposable to that of Dukes' type C SW620, demonstrating a tmCLIC1 fluorescence significantly higher compared to non-cancerous cell line CCD841, but a level of fluorescence significantly lower to that of the most aggressive cell line COLO201. At the same time, MC38 cell line has demonstrated a level of tmCLIC1-dependent fluorescence significantly higher compared to other human CRCs, except COLO201, and to the other murine colorectal cancer cell line, CT26.

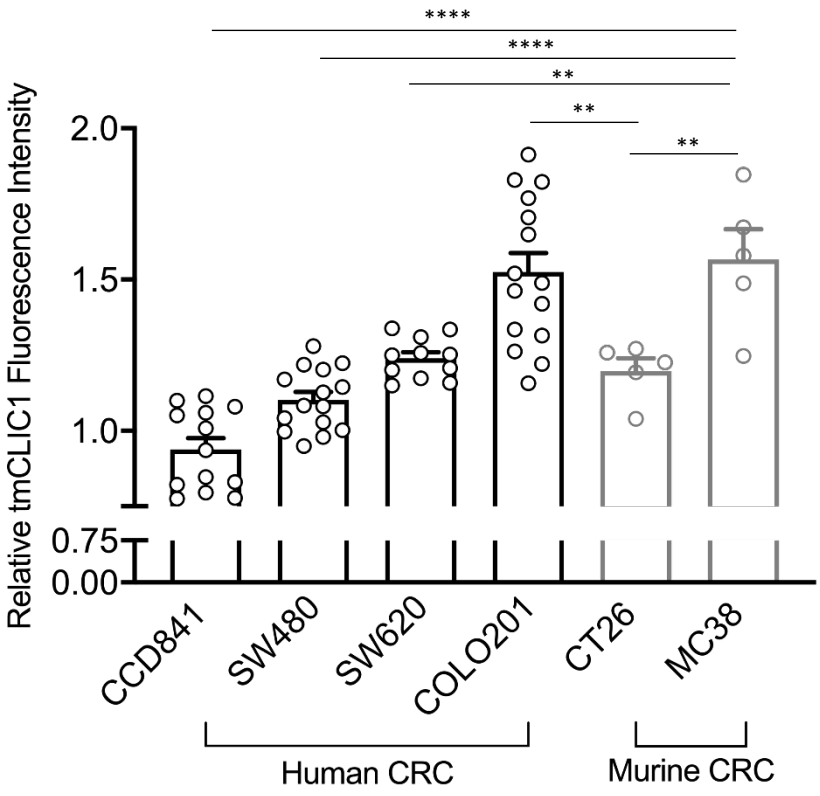

Figure 26. Fluorescence intensity assay of human colorectal cancer cells in comparison to murine colorectal cancer cells. CT26 have demonstrated a significantly higher tmCLIC1 fluorescence compared to non-cancerous cell CCD841 (One-way ANOVA, * CCD841 vs CT26, p=0.0342, n=5), while has lower fluorescence compared to the most aggressive cell line COLO201 (One-way ANOVA, ** COLO201 vs CT26, p=0.0026). MC38 cell line shows the highest level of fluorescence intensity, superimposable to what is visible in COLO201 (One-way ANOVA, **** CCD841 vs MC38, p<0.0001; **** SW480 vs MC38, p<0.0001, ** SW620 vs MC38, p=0.0044; n=5), and a significantly higher tmCLIC1 fluorescence compared to CT26 (One-way ANOVA, ** CT26 vs MC38, p=0.0069 n=5; Tukey's multiple comparison test).

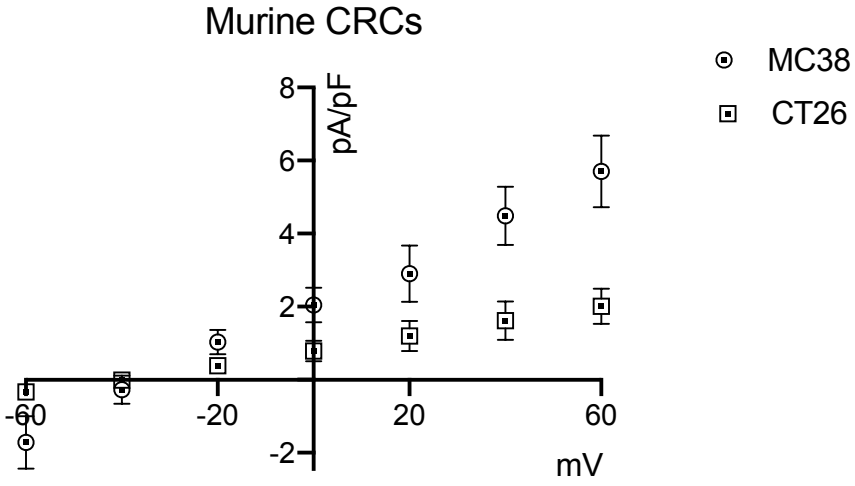

Figure 27. Electrophysiology experiments in perforated patch clamp configuration on murine colorectal cancer cells CT26 (pointed clear squares), and MC38 (pointed clear circles). Cells line have not demonstrated significantly differences in tmCLIC1- mediated current.

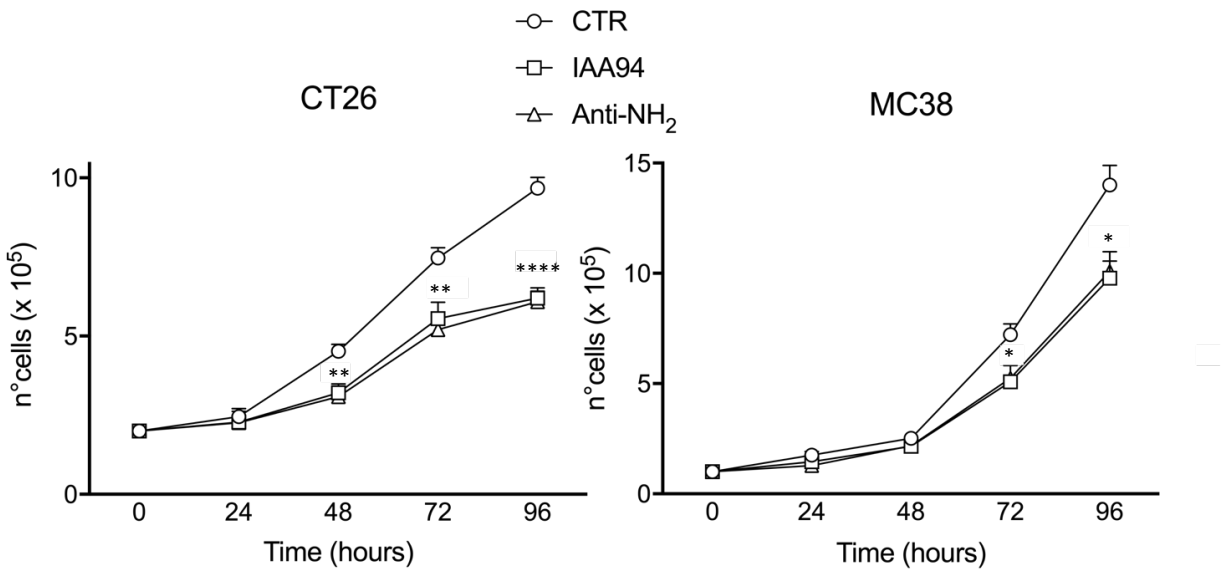

Figure 28. Growth curves experiments on murine colorectal cancer cell lines CT26 (right) and MC38 (left) in the absence (clear circles) and presence of IAA94 (clear squares) and Anti-NH_2 (clear triangle) from 0 to 96 hours. In CT26, treatments impair proliferation of cells significantly after just 48h of culture (One-way ANOVA, 48h: ** CTR vs IAA94 and Anti-NH_2, p=0.0020, p=0.0028; 72h: ** CTR vs IAA94 and Anti-NH_2, p=0.0021, p=0.0019; 96h: **** CTR vs IAA94, Anti-NH_2; p<0.0001, Dunnett's multiple comparison test, n=6). MC38 cell line has demonstrated a significantly downregulation of proliferation in the presence of both IAA94 and Anti-NH_2 after 72h of treatment (One-way ANOVA, 72h: * CTR vs IAA94, and Anti-NH_2, p=0.0330, p=0.0293; 96h: * CTR vs IAA94, and Anti-NH_2, p=0.0109, p=0.0171, Dunnett's multiple comparison test n=7)

To associate the presence of tmCLIC1 in plasma membrane to its activity as a chloride channel, electrophysiology experiments in murine colorectal cancer cells were performed. As a result, as is shown in Figure 27, CT26 and MC38 have demonstrated no significant differences in tmCLIC1-mediated current. Next, we examined the proliferation of both CT26 and MC38 in the absence or presence of the tmCLIC1 inhibitors IAA94, and anti-NH_2 from 0 to 96 hours. The Figure 28 shows that in CT26 cell line the proliferation is significantly impaired starting from 48h of culture in the presence of both treatments, while in MC38 the growth rate is significantly impaired after 72h of treatments, demonstrating that also in murine colorectal cancer cells tmCLIC1 activity has a pivotal role in tumor progression.

As for human colorectal cancer cells, the migration and invasion potential of murine cells was analyzed in the absence or presence of tmCLIC1 inhibitors. After 72h of treatments membranes were stained with DAPI to mark migrating and invasive nuclei. The Figure 29 depicted the results obtained in both CT26 and MC38 for invasion and migration assays. CT26 cell lines has demonstrated that in the presence of IAA94 and tmCLIC1omab (the antibody used for all the experiments in the present work, now under license) the number of migrative and invasive nuclei is significantly impaired. In MC38, the results obtained have demonstrated that also in this cell line the treatments can impair significantly both invasion and migration. All these results have demonstrated that tmCLIC1 role has a fundamental role not only in human colorectal cancer cells, but also in murine colorectal cancer cells.

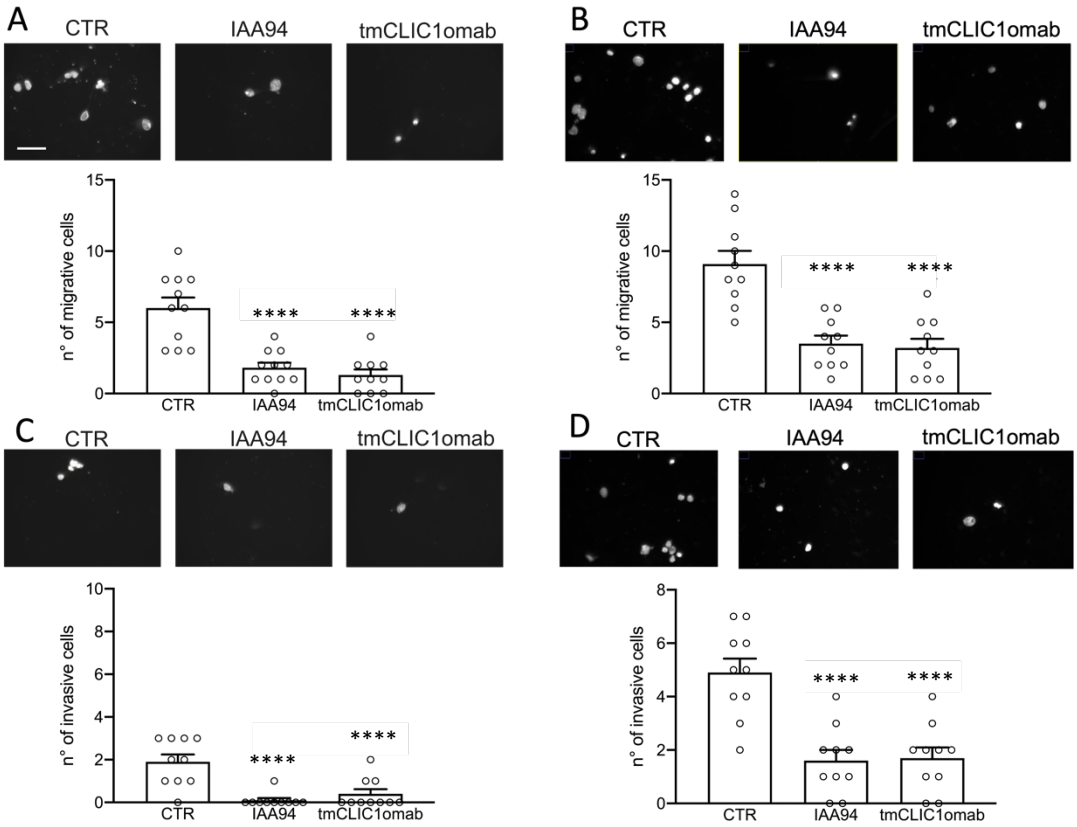

Figure 29. Trans well assay for evaluation of migration and invasion potential of CT26 and MC38 cells. A) Migration assay of CT26 cells. After 72h of treatment both IAA94 and tmCLIC1omab are able to significantly impair the number of migrative cells (One-way ANOVA, **** CTR vs IAA94 and tmCLIC1omab, $p<0.0001$, Tukey's multiple comparison test, n=11). B) Migration assay of MC38 cell line. The number of invasive nuclei is significantly lower after treatments (One-way ANOVA, **** CTR vs IAA94 and tmCLIC1omab, $p<0.0001$, Tukey's multiple comparison test, n=10). C) Invasion assay of CT26 cell lines after 72h of treatment. Invasive nuclei are mainly absent in the presence of treatments (One-way ANOVA, **** CTR vs IAA94 and tmCLIC1omab, $p<0.0001$, Tukey's multiple comparison test, n=10). D) Invasion assay of MC38 cells. After 72h of culture the number of invasive nuclei is significantly impaired in treated cells compared to control (One-way ANOVA, **** CTR vs IAA94 and tmCLIC1omab, $p<0.0001$, Tukey's multiple comparison test, n=11). Scale bar: 20uM.

4.9 Knockdown of CLIC1 in murine colorectal cancer affects tumorigenesis in immunocompetent mice

Murine colorectal cancer cells have demonstrated a phenotype superimposable to what was shown in human CRCs, with the same role of tmCLIC1 activity in tumorigenesis. In this scenario, we performed a pilot study on immunocompetent mice. Experiments were performed first with MC38 that have demonstrated a more aggressive phenotype compared to CT26. First, cells were engineered to obtain a stable CLIC1-knockdown cell line, then selected through cell sorting. $2x10^5$ cells were injected in the rectum of C57BL/6 BALB/6 mice, after two weeks was possible to visualize tumors in the rectum. After 18 days, mice were sacrificed, tumors were weighted, and their volume was measured.

In Figure 30 is visible that after 18 days the tumor volume of SCR cells was significantly higher compared to shCLIC1 cancers. Only two mice injected with shCLIC1 cells, indeed, have shown a minimal tumor mass. Rectum of mice were explanted, weighted, and included in OCT to perform immunofluorescence experiments (data not shown). Mesenteric and iliac lymph nodes were removed and weighted, to evaluate whether an inflammation occurs in mice injected with colorectal cancer cells also. As represented in Figure 31, rectum of mice injected with SCR cells have demonstrated a significantly higher weight compared to rectum of mice injected with shCLIC1 cells, as expected. At the same time, mesenteric lymph nodes weight was almost the same between SCR and shCLIC1 mice. On the contrary, iliac lymph nodes have demonstrated a significant higher weight in SCR mice compared to shCLIC1 mice. This phenomenon is probably due to the manifestation of a higher inflammation in mice that have demonstrated the presence of tumors. After the sacrifice, we also analyzed the presence of metastases in kidneys and lungs. After the homogenizations, cells were examined through FACS experiments to visualize the presence of ZsGreen cells in organs. We observed that 18 days were not sufficient to visualize any metastases formation (data not shown). Therefore, we are now performing experiments in which the end point is fixed after 40 days post injection. Moreover, we are performing

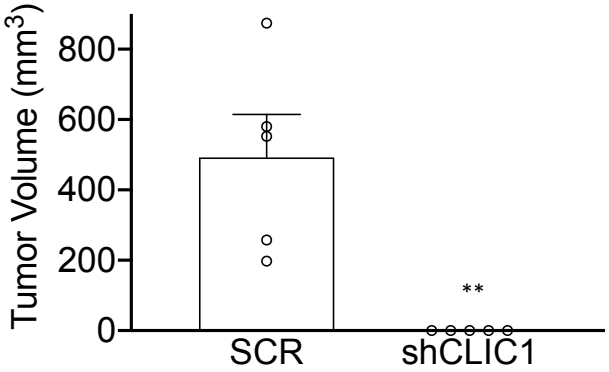

Figure 31. Tumor volume of SCR and shCLIC1 MC38 after 18 days post injection. As is visible, the volume of SCR tumors is significantly higher compared to shCLIC1 tumors. In particular, only 2/5 mice injected with shCLIC1 shown tumor formation (Student's t test, ** SCR vs shCLIC1, p=0.0038, n=5

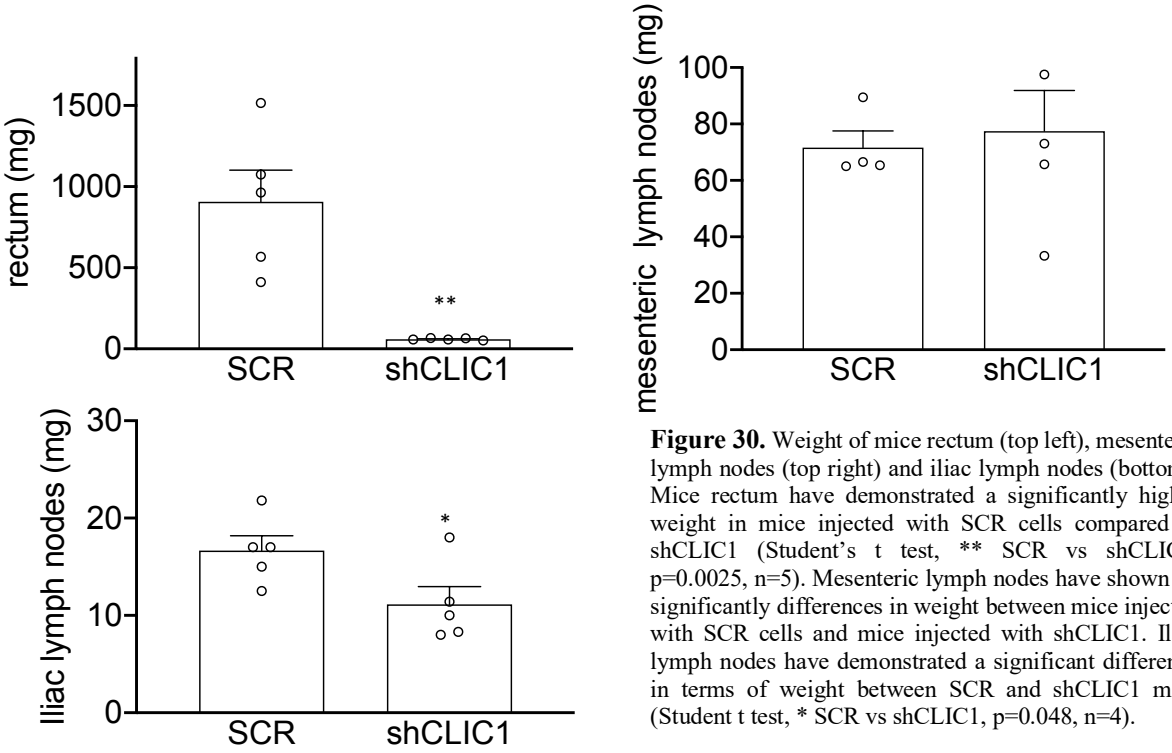

Figure 30. Weight of mice rectum (top left), mesenteric lymph nodes (top right) and iliac lymph nodes (bottom). Mice rectum have demonstrated a significantly higher weight in mice injected with SCR cells compared to shCLIC1 (Student's t test, ** SCR vs shCLIC1, p=0.0025, n=5). Mesenteric lymph nodes have shown no significantly differences in weight between mice injected with SCR cells and mice injected with shCLIC1. Iliac lymph nodes have demonstrated a significant difference in terms of weight between SCR and shCLIC1 mice (Student t test, * SCR vs shCLIC1, p=0.048, n=4).

experiments in which mice are treated with our tmCLIC1omab to verify whether the antitumoral proprieties seen *in vitro* are also confirmed *in vivo*.

4.10 tmCLIC1 mechanism of action in metastatic processes

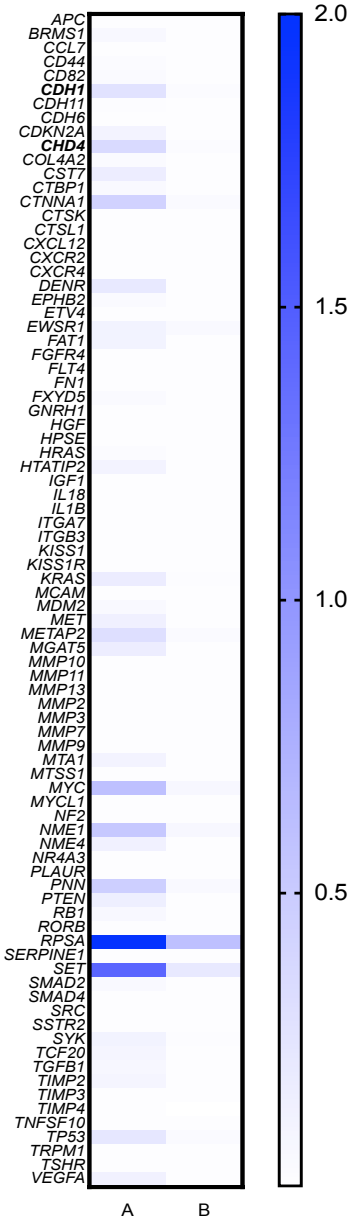

Figure 32. RT PCR of 88 genes involved in metastatic processes in COLO201 SCR (A) and sh3 (B). Different genes have demonstrated downregulated expression.

At this point, a question is still present. How CLIC1 could alter the proliferation and metastatic processes in colorectal cancer? To have a primary idea of the mechanism of action, we made preliminary experiment performing a RT PCR on metastatic pathways in COLO201 SCR and sh3. Figure 32 shows a huge panel of 88 genes in which was demonstrated that there is a down regulation of expression of pro metastatic genes CDH1, CHD4, SET, RPSA, CTNNA1, and more. Most of these genes are modulated by Reactive Species of Oxygen (ROS) level. CLIC1 was found to be essential in ROS, regulating the activity of NADPH oxidase (Peretti). In literature is reported that, surprisingly, metastatic cells have demonstrated a high level of the antioxidant Glutathione (GSH) and high level of ROS (Nature, oxidative stress). CLIC1 in its cytoplasmic form is complexed with GSH. After oxidation and pH alteration, CLIC1 releases GSH in cytoplasm and translocate to plasma membrane where supports ROS overproduction. In this scenario, our idea was that CLIC1 supports tumorigenesis releasing GSH that work as antioxidant. At the same time, the expression of CLIC1 in plasma membrane supports the production of ROS and, consequently, the promotion of proliferation and metastatic pathways. To confirm our idea, we used the Dukes' type B cell line

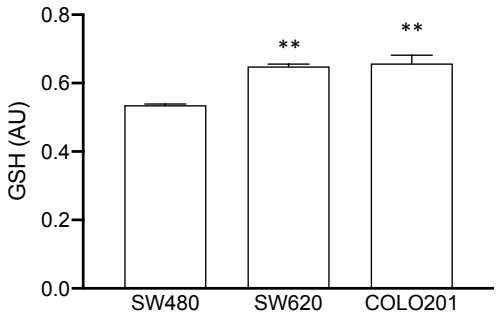

Figure 33. GSH measurements in CRCs. The most aggressive cell lines SW620 and COLO201 have demonstrated a significantly higher level of GSH compared to non-metastatic SW480 (One-way ANOVA, ** SW480 vs SW620, p=0.0024; ** SW480 vs COLO201, p=0.0017; Dunnett's multiple comparison

SW480, to understand whether the release of GSH is depending on the increase of tmCLIC1 in plasma membrane and enhance the proliferation rate and invasion potential of cells that normally do not form metastases. GSH was measured in SW480, SW620, and COLO201). Unexpectedly, the antioxidant GSH was found to be significantly higher in the most aggressive cell lines SW620 and COLO201 compared to non-metastatic cells SW480 (Figure 33). In order to verify whether a large amount of GSH corresponds to an increase of tmCLIC1 expression and activity, was used a drug for the release of GSH, the N- Acetyl- Cysteine (NAC) in the non-metastatic colorectal cancer cells SW480, since have demonstrated a low rate of tmCLIC1 expression. First, was performed a dose-response experiment to assess NAC working concentration. After 72 h, cells were counted and as depicted in Figure 31, the proliferation of SW480 in the presence of low doses of NAC is incremented, while decrease at higher dose of NAC. Therefore, we used 0.3 mM of NAC to perform the next experiments. Next, we evaluated if tmCLIC1 increases after the treatment with NAC performing fluorescence intensity assay and patch clamp experiments.

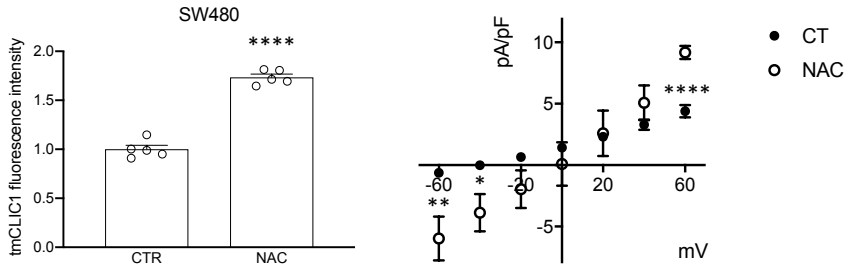

Figure 34. Fluorescence intensity assay (left) and patch clamp experiments (right) on SW480 in the absence or presence of NAC. In the presence of NAC, tmCLIC1 fluorescence is significantly increased compared to control (Student's t test, **** CTR vs NAC, $p<0.0001$, n=5). In electrophysiology experiments, in the presence of NAC tmCLIC1-mediated current is significantly higher compared to control (Student's t test, -60 mV: **, $p=0.0076$; -40mV: *, $p=0.0179$; +60 mV: ****, $p<0.0001$, n=7)

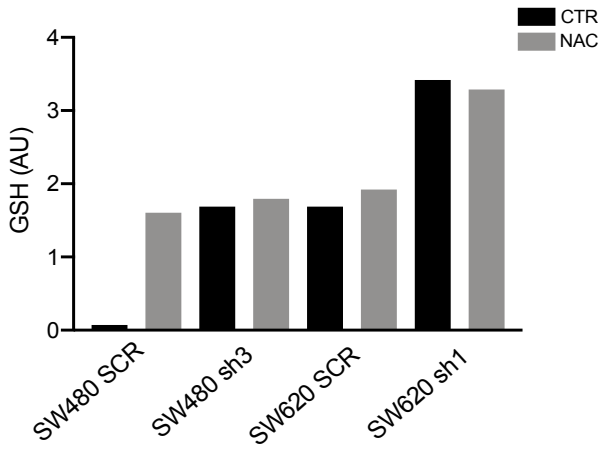

Figure 35. GSH assay performed of SW480 and SW620 in SCR and silenced clones in the absence (black histogram) or presence (grey histogram) of NAC. SW480 SCR have demonstrated a low level of GSH, but this increase after treatment with NAC. SW480 sh3 cells demonstrate a higher level of GSH that does not increase after culture with NAC. SW620 SCR cells show a similar level of GSH to what is seen in SW480 sh3, and the treatment of NAC does not increase GSH level. On the contrary, SW620 sh1 have demonstrated the highest level of GSH that is not altered by treatment with NAC.

In Figure 34 is shown how tmCLIC1 increases its expression and activity when cells are treated with NAC. To evaluate what happen when CLIC1 is silenced, we measured the GSH level in colorectal cancer cells SW480 and SW620 in SCR and sh conditions. It was impossible to perform this experiment in COLO201 since NAC results extremely toxic in these cells. As a result, Figure 35 shows how NAC treatment increases the level of GSH in SW480 SCR cells, while in SW480 sh3 the level of GSH is higher, similar to that of SCR cells under NAC treatment, and is not affected by NAC.

Surprisingly, in SW620 SCR the level of GSH is higher compared to SW480 SCR, similar to that of SW480 sh3. In SW620 sh1, the level of GSH is the highest, and is not altered under NAC treatment. The explanation of this phenomenon could be that in sh cells CLIC1 protein is not expressed, and probably GSH is not complexed with cytosolic CLIC1 and is free in cytoplasm. Considering that in this work was demonstrated that the high level of tmCLIC1 expression results in a more aggressive phenotype of colorectal cancer cells, and that NAC increase tmCLIC1 expression, we want to verify whether the migration and invasion potential of non-metastatic cells increased after NAC treatment. Cells were plated onto Trans well support in the absence or presence of 0.3 mM of NAC. We evaluated the number of migrative and invasive nuclei. As represented in Figure 36, in control conditions cells were not able to migrate and invade across the membrane. On the contrary, in the presence of NAC, a huge number of cells were detected in permeable membranes. These experiments are a starting point to study more in deep the mechanism of action of tmCLIC1 modulating the content of GSH molecule in cellular cytoplasm and promoting, at the same time, the overproduction of ROS that are the key regulator for proliferation and metastasis pathways. We have planned to performed experiments to confirm this trend in cells that are silenced for CLIC1 protein.

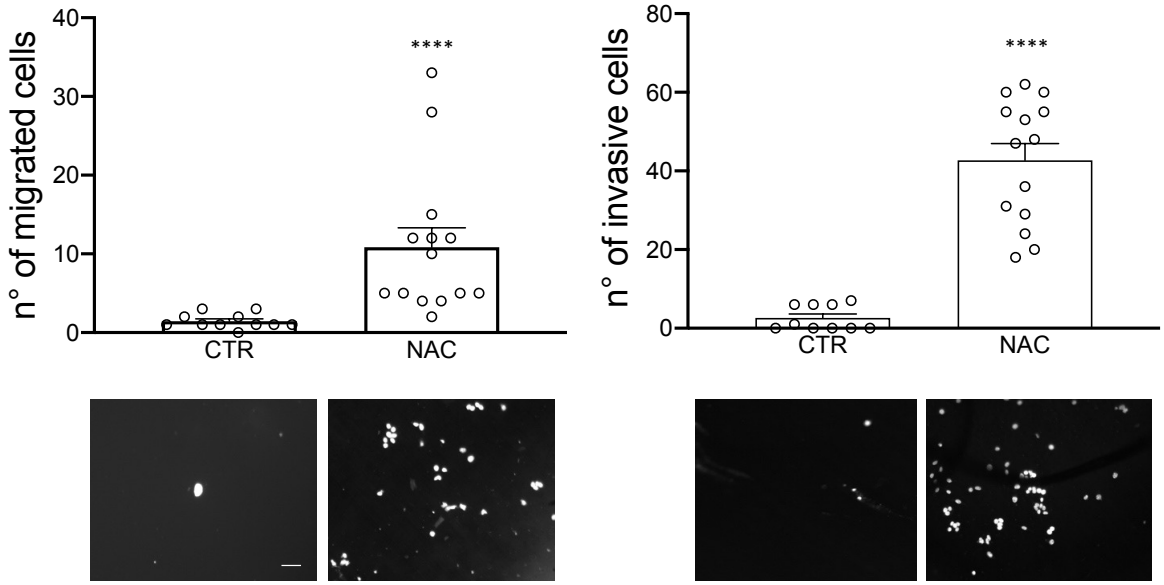

Figure 36. Trans well assay on migration (left) and invasion (right) potential of SW480 cells in control and after NAC treatment. In migration assay is visible that the number of migrating nuclei is significantly higher after the treatment with NAC (Student's t test, ** CTR vs NAC; p=0.0029, unpaired test). In invasion assay the number of invasive nuclei in significantly increased after the NAC treatment (Student's t test, **** CTR vs NAC, p<0.001, unpaired test). Scale bar: 20um

5. Discussion

All the living organisms constantly rely in a dynamic state of equilibrium defined as homeostasis. When a stress stimulus occurs, cells activate specific pathways called allostatic mechanisms that respond to stress restoring homeostasis. When stress stimuli became persistent, the hyperactivation of allostatic mechanisms results, in most of the cases, in cell death. Alternatively, the chronic activation of these pathways results in the establishment in a new homeostatic state, called allostasis. Cancer cells reside in allostasis and form a new cellular population, characterized by the hyperactivation of cellular pathways that promote cancer development, proliferation, and metastasis. Ion channels altered activity is extremely important in tumorigenesis, making them the ideal target for antitumoral therapies. The main problem is that a major part of ion channels is involved in all normal cellular functions, and its inhibition could result in strong toxicity. Therefore, an ideal therapeutic approach must be specific for cancer cells. CLIC1 protein could be considered a promising target to achieve this purpose. Although CLIC1 was found to be overexpressed in different solid tumors and correlated to a poor prognosis, its mechanism of action in tumorigenesis and cancer development hasn't been described yet. Our laboratory has demonstrated that glioblastoma stem cells are characterized by the chronic presence of the transmembrane form of CLIC1 protein (tmCLIC1) that has a pivotal role in cancer sustainment. CLIC1 is overexpressed in numerous solid tumors, particularly in the most aggressive. Colorectal cancer is one of the leading cancer-related death worldwide. When is diagnosed in the early stage of development could be efficiently eradicated through surgical intervention and chemo- and radiotherapies; but, in the presence of metastases, remains still uncurable. CLIC1 mRNA was found to be overexpressed in colorectal cancer cells, especially in the presence of metastasis. The correlation between metastatic potential and CLIC1 expression is not clarified yet, therefore, the main aim of the present work is to study the role of CLIC1 protein in colorectal cancer development and in the acquirement of aggressive phenotype. We have evaluated the level of expression of CLIC1 in four different human immortalized colorectal cancer cells (CRCs), chosen at different stage of aggressiveness according to the Dukes' classification. The Dukes' staging is a method of classification of CRCs that consider cellular invasion of mucosa and bowel. We used a normal epithelium cell line, the CCD841, as a control, the Dukes' type B SW480 that are tumor cells that invade mucosa without the involvement of lymph nodes. As aggressive cells were used SW620, characterized by lymph nodes metastasis (Dukes type C); and COLO201, the Dukes type D, in which are present

widespread metastases. Although the mRNA level is similar in all mentioned cell lines, except in COLO201 (Figure 5), the expression of the protein seen through western blot analysis is proportional to the level of aggressiveness of CRCs, as is shown in Figure 6. Considering the metamorphism of CLIC1 and its role as a chloride channel, we investigated whether the overexpression of the protein is related to increased activity as a chloride channel in plasma membrane of CRCs. As is depicted in Figure 7, from fluorescence intensity assays and electrophysiological experiments, the transmembrane form of CLIC1 is enriched in aggressive cells. Moreover, tmCLIC1-mediated current is significantly higher in Dukes' type C SW620 and Dukes' type D COLO201, demonstrating that the activity of tmCLIC1 protein is correlated to aggressive phenotype. To confirm this, the proliferation of CRCs and the epithelium control was evaluated in the presence of tmCLIC1 inhibitors. Were used IAA94, the specific tmCLIC1 blocker, and a monoclonal antibody designed in our laboratory to specifically recognized the NH_2 domain of CLIC1 that is exposed to the extracellular space when the protein is docked in membrane. We decided to design a new antibody, that now is under license, because IAA94 has demonstrated high toxicity *in vivo*. Our antibody, registered as tmCLIC1omab, has demonstrated good proprieties detecting exclusively the transmembrane form of CLIC1 and impairing its functional activity. Moreover, as is represented in Figure 8, the inhibition of tmCLIC1 activity through both IAA94 and tmCLIC1omab is superimposable, and results in a significant impairment of cancer cells' growth, while has no effect on normal epithelium cells. As expected, the proliferation is significantly affected in SW620 and COLO201, the most aggressive lines, after 72 and 48 hours of treatment, respectively. This trend was confirmed also in 3D models, demonstrating that inhibitors can infiltrate the spheroids (Figure 9). TmCLIC1 activity was found to be correlated in G1/S phase transition of cell cycle (Figure 11), and its inhibition results in the accumulation of cells in G1 phase (Figure 12). The inhibitors of tmCLIC1 have demonstrated a very good specificity, considering that the experiments replicated in cells engineered to stable knockdown CLIC1 protein expression, have demonstrated the same results obtained after treatments with both IAA94 and tmCLIC1omab (Results; point 4.3). Moreover, the migration and invasion potential of cells treated with tmCLIC1 inhibitors is significantly affected, as well as cells in which CLIC1 was silenced *in vitro* (Figure 17 and 18). At the same time, the expression of two of the most important proteins involved in migration and invasion mechanisms is mainly abolished in the presence of both IAA94 and tmCLIC1omab (Figure 19). Our investigation was applied also in *in vivo* models. First, SCR controls and sh cells were injected in the perivitelline space of Zebrafish embryos. This model is extremely useful to evaluate the proliferation of tumors and the formation of metastases. In perivitelline space tumors can create a new network

of vascularization that can promote the migration of cells in other sites distant from primary tumors. In zebrafish embryos injected with silenced CLIC1 cells not only was demonstrated that the primary tumors have a significantly lower density compared to the SCR controls, but also that in the absence of CLIC1 expression, tumors are not able to form metastases (Figure 20, 21, and 23). Experiments performed in immunodeficient mice with COLO201 have demonstrated that silenced sh3 tumor proliferation is significantly impaired compared to SCR tumors, while, although sh1 tumors have demonstrated the same growth rate of SCR tumors (Figure 23), the percentage of disseminating tumor cells in mice lungs is significantly lower in both silenced tumors compared to control (Figure 24). These results demonstrate that it does not exist necessarily a correlation between tumors' proliferation rate and their metastatic potential. Performing a RT PCR on COLO201 SCR and sh cells on 88 genes of metastasis, we noticed that in sh cells the expression of genes that are modulated by ROS level results downregulated (Figure 32). CLIC1 protein was found to support the ROS overproduction of tumor cells with a feedforward mechanism with NADPH oxidase and NHE1 proton pump [62]. This do not explain why tmCLIC1 translocate to the plasma membrane and is chronically expressed in tumor cells. Recently, it has been demonstrated that metastatic melanoma cells have shown a high level of cytoplasmic reduced glutathione (GSH) molecule [88]. GSH is an antioxidant molecule that prevent cellular damage neutralizing and reducing the amount of cellular ROS. CLIC1 protein contains a GSH binding site at the level of NH_2 domain that binds GSH when is expressed in its cytosolic monomeric form. Under stress condition, the high level of ROS causes a conformational change in the NH_2 domain of CLIC1 protein, and the consequent release of GSH in cytoplasm [53]. Our main idea is that in cancer cells the microenvironment characterized by strong acidification of pH and the increased ROS level, leads to the release of GSH molecule in cytoplasm as a defensive mechanism. At the same time, the insertion of tmCLIC1 in plasma membrane of cancer cells promotes the overproduction of ROS and the consequent sustainment of abnormal proliferation and invasive mechanisms. To confirm our hypothesis, were performed preliminary experiments. First, was measured GSH level in the cytoplasm of the human CRCs. According to our hypothesis, the most aggressive cell lines SW620 and COLO201 have demonstrated a significantly higher level of GSH in their cytoplasm. Now our question was: what happen if we force GSH release in non-metastatic colorectal cancer cells? To this purpose, we decided to treat SW480 cells with N-Acetyl-Cysteine (NAC), an antioxidant that act stimulating the GSH release in cytoplasm. After treatment with NAC, SW480 cells have demonstrated a significant enrichment of tmCLIC1 expression and activity (Figure 34). Next, to evaluate what happen to GSH release when CLIC1 protein is absent, we stimulated SW480 and SW620 cell line in SCR

and sh conditions with NAC, measuring the level of GSH in cytoplasm. SW480 SCR cells treated with NAC have demonstrated a GSH level significantly higher compared to the untreated control. In SW480 sh3 cells the basal GSH amount in cytoplasm is higher compared to SCR control while here the amount of GSH remains constant in control after the treatment with NAC. This could be explained by the fact that the absence of CLIC1 results in free GSH that is not complexed with the protein, confirming that the consequent release of GSH is dependent by CLIC1 presence. GSH was measured also in the more aggressive cell line SW620, that is characterized by a significantly higher expression of tmCLIC1 protein compared to SW480. SW620 cells have demonstrated a basal level of GSH higher compared to SW480, probably because the CLIC1 protein is expressed as a transmembrane ion channel, and not as cytosolic monomer complexed with GSH. In these cells, NAC treatment does not significantly improve the amount of GSH, considering that they are already metastatic and aggressive. SW620 sh3 clone has demonstrated a huge amount of free GSH, that is not improved by NAC treatment. Also in this case, our thoughts were that absence of CLIC1 protein expression causes a huge amount of free GSH that is not complexed with our protein of interest. Moreover, the presence of antioxidants in cytoplasm of these cells could explain their phenotype and the downregulation on tumor proliferation, migration, and invasion. All these experiments must be supplemented; but these preliminary trials are a starting point to validate our idea. Additionally, we evaluated whether the release of GSH derived from translocation of CLIC1 in plasma membrane could promote the acquirement of metastatic phenotype. SW480 cells are cancer cells that do not invade either lymph nodes or other distal sites. We performed Trans well experiments for the assessment of migration and invasion potential of cells in absence or presence of NAC. After 72h of treatment, cells incubated with NAC have demonstrated a significantly higher number of both migrative and invasive nuclei, while in control conditions the number of nuclei is negligible (Figure 36). This evidence demonstrates that tmCLIC1 expression and activity is essential for the acquirement of aggressive phenotype. In conclusion, this work has demonstrated that the impairment of tmCLIC1 activity results in a downregulation of tumor proliferation *in vitro* as well as *in vivo* models, as zebrafish embryos and murine models. This result was confirmed also in immunocompetent mice injected with murine CRCs that have demonstrated the same phenotype of human CRCs (Results, point 4.7 and 4.8). For the first time, in the present work we tried to explain a cancer physiological phenomenon, that concern an allostatic mechanism in response to stress stimuli that establishes a new homeostatic state typical of pathological conditions. In this scenario, the inhibition of these pathways could represent a new therapeutical strategy to counteract against metastatic cancers, that now remains uncurable. Our monoclonal antibody

with its strong propriety in inhibition of tmCLIC1 activity *in vitro*, could be considered a promising adjuvant therapy for the treatment of metastatic colorectal cancer cells, blocking their migrative and invasive potential. To this purpose we are now studying its proprieties *in vivo* using a murine model, to translate its utilization in humans as soon as possible.

6. Bibliography

1 Burt, R. W. Colon cancer screening. *Gastroenterology* **119**, 837-853, doi:10.1053/gast.2000.16508 (2000).

2 Fearon, E. R. & Vogelstein, B. A genetic model for colorectal tumorigenesis. *Cell* **61**, 759-767, doi:10.1016/0092-8674(90)90186-i (1990).

3 De Rosa, M. *et al.* Genetics, diagnosis and management of colorectal cancer (Review). *Oncol Rep* **34**, 1087-1096, doi:10.3892/or.2015.4108 (2015).

4 Pancione, M., Remo, A. & Colantuoni, V. Genetic and epigenetic events generate multiple pathways in colorectal cancer progression. *Patholog Res Int* **2012**, 509348, doi:10.1155/2012/509348 (2012).

5 Beckman, R. A. & Loeb, L. A. Genetic instability in cancer: theory and experiment. *Semin Cancer Biol* **15**, 423-435, doi:10.1016/j.semcancer.2005.06.007 (2005).

6 Pino, M. S. & Chung, D. C. The chromosomal instability pathway in colon cancer. *Gastroenterology* **138**, 2059-2072, doi:10.1053/j.gastro.2009.12.065 (2010).

7 Smith, G. *et al.* Mutations in APC, Kirsten-ras, and p53--alternative genetic pathways to colorectal cancer. *Proc Natl Acad Sci U S A* **99**, 9433-9438, doi:10.1073/pnas.122612899 (2002).

8 Boland, C. R. & Goel, A. Microsatellite instability in colorectal cancer. *Gastroenterology* **138**, 2073-2087 e2073, doi:10.1053/j.gastro.2009.12.064 (2010).

9 Hughes, L. A. *et al.* The CpG island methylator phenotype in colorectal cancer: progress and problems. *Biochim Biophys Acta* **1825**, 77-85, doi:10.1016/j.bbcan.2011.10.005 (2012).

10 Toyota, M. *et al.* CpG island methylator phenotype in colorectal cancer. *Proc Natl Acad Sci U S A* **96**, 8681-8686, doi:10.1073/pnas.96.15.8681 (1999).

11 Nazemalhosseini Mojarad, E., Kuppen, P. J., Aghdaei, H. A. & Zali, M. R. The CpG island methylator phenotype (CIMP) in colorectal cancer. *Gastroenterol Hepatol Bed Bench* **6**, 120-128 (2013).

12 Sinicrope, F. A. *et al.* Prognostic impact of microsatellite instability and DNA ploidy in human colon carcinoma patients. *Gastroenterology* **131**, 729-737, doi:10.1053/j.gastro.2006.06.005 (2006).

13 Vatandoust, S., Price, T. J. & Karapetis, C. S. Colorectal cancer: Metastases to a single organ. *World J Gastroenterol* **21**, 11767-11776, doi:10.3748/wjg.v21.i41.11767 (2015).

14 Smothers, L. *et al.* Emergency surgery for colon carcinoma. *Dis Colon Rectum* **46**, 24-30, doi:10.1007/s10350-004-6492-6 (2003).

15 Chapuis, P. H. *et al.* A multivariate analysis of clinical and pathological variables in prognosis after resection of large bowel cancer. *Br J Surg* **72**, 698-702, doi:10.1002/bjs.1800720909 (1985).

16 Rosen, R. D. & Sapra, A. in *StatPearls* (2021).

17 Akkoca, A. N. *et al.* TNM and Modified Dukes staging along with the demographic characteristics of patients with colorectal carcinoma. *Int J Clin Exp Med* **7**, 2828-2835 (2014).

18 Chau, I. & Cunningham, D. Treatment in advanced colorectal cancer: what, when and how? *Br J Cancer* **100**, 1704-1719, doi:10.1038/sj.bjc.6605061 (2009).

19 Legolvan, M. P., Taliano, R. J. & Resnick, M. B. Application of molecular techniques in the diagnosis, prognosis and management of patients with colorectal cancer: a practical approach. *Hum Pathol* **43**, 1157-1168, doi:10.1016/j.humpath.2012.03.003 (2012).

20 Bouvier, A. M. *et al.* Incidence and patterns of late recurrences in colon cancer patients. *Int J Cancer* **137**, 2133-2138, doi:10.1002/ijc.29578 (2015).

21 Yogi, A., O'Connor, S. E., Callera, G. E., Tostes, R. C. & Touyz, R. M. Receptor and nonreceptor tyrosine kinases in vascular biology of hypertension. *Curr Opin Nephrol Hypertens* **19**, 169-176, doi:10.1097/MNH.0b013e3283361c24 (2010).
22 Gabashvili, I. S., Sokolowski, B. H., Morton, C. C. & Giersch, A. B. Ion channel gene expression in the inner ear. *J Assoc Res Otolaryngol* **8**, 305-328, doi:10.1007/s10162-007-0082-y (2007).
23 Littleton, J. T. & Ganetzky, B. Ion channels and synaptic organization: analysis of the Drosophila genome. *Neuron* **26**, 35-43, doi:10.1016/s0896-6273(00)81135-6 (2000).
24 Bose, T., Cieslar-Pobuda, A. & Wiechec, E. Role of ion channels in regulating Ca(2)(+) homeostasis during the interplay between immune and cancer cells. *Cell Death Dis* **6**, e1648, doi:10.1038/cddis.2015.23 (2015).
25 Berridge, M. J., Lipp, P. & Bootman, M. D. The versatility and universality of calcium signalling. *Nat Rev Mol Cell Biol* **1**, 11-21, doi:10.1038/35036035 (2000).
26 Bates, E. Ion channels in development and cancer. *Annu Rev Cell Dev Biol* **31**, 231-247, doi:10.1146/annurev-cellbio-100814-125338 (2015).
27 Brahimi-Horn, M. C. & Pouyssegur, J. Oxygen, a source of life and stress. *FEBS Lett* **581**, 3582-3591, doi:10.1016/j.febslet.2007.06.018 (2007).
28 Gatenby, R. A. & Gillies, R. J. A microenvironmental model of carcinogenesis. *Nat Rev Cancer* **8**, 56-61, doi:10.1038/nrc2255 (2008).
29 Vaupel, P. Tumor microenvironmental physiology and its implications for radiation oncology. *Semin Radiat Oncol* **14**, 198-206, doi:10.1016/j.semradonc.2004.04.008 (2004).
30 Hanahan, D. & Weinberg, R. A. Hallmarks of cancer: the next generation. *Cell* **144**, 646-674, doi:10.1016/j.cell.2011.02.013 (2011).
31 Leanza, L. *et al.* Intracellular ion channels and cancer. *Front Physiol* **4**, 227, doi:10.3389/fphys.2013.00227 (2013).
32 Pardo, L. A. & Stuhmer, W. The roles of K(+) channels in cancer. *Nat Rev Cancer* **14**, 39-48, doi:10.1038/nrc3635 (2014).
33 Hoffmann, E. K. & Lambert, I. H. Ion channels and transporters in the development of drug resistance in cancer cells. *Philos Trans R Soc Lond B Biol Sci* **369**, 20130109, doi:10.1098/rstb.2013.0109 (2014).
34 Litan, A. & Langhans, S. A. Cancer as a channelopathy: ion channels and pumps in tumor development and progression. *Front Cell Neurosci* **9**, 86, doi:10.3389/fncel.2015.00086 (2015).
35 Cuddapah, V. A. & Sontheimer, H. Ion channels and transporters [corrected] in cancer. 2. Ion channels and the control of cancer cell migration. *Am J Physiol Cell Physiol* **301**, C541-549, doi:10.1152/ajpcell.00102.2011 (2011).
36 Prevarskaya, N., Skryma, R. & Shuba, Y. Ion channels and the hallmarks of cancer. *Trends Mol Med* **16**, 107-121, doi:10.1016/j.molmed.2010.01.005 (2010).
37 Peretti, M. *et al.* Chloride channels in cancer: Focus on chloride intracellular channel 1 and 4 (CLIC1 AND CLIC4) proteins in tumor development and as novel therapeutic targets. *Biochim Biophys Acta* **1848**, 2523-2531, doi:10.1016/j.bbamem.2014.12.012 (2015).
38 Setti, M. *et al.* Functional role of CLIC1 ion channel in glioblastoma-derived stem/progenitor cells. *J Natl Cancer Inst* **105**, 1644-1655, doi:10.1093/jnci/djt278 (2013).
39 Wang, P. *et al.* Chloride intracellular channel 1 regulates colon cancer cell migration and invasion through ROS/ERK pathway. *World J Gastroenterol* **20**, 2071-2078, doi:10.3748/wjg.v20.i8.2071 (2014).
40 Valenzuela, S. M. *et al.* Molecular cloning and expression of a chloride ion channel of cell nuclei. *J Biol Chem* **272**, 12575-12582, doi:10.1074/jbc.272.19.12575 (1997).

41 Heiss, N. S. & Poustka, A. Genomic structure of a novel chloride channel gene, CLIC2, in Xq28. *Genomics* **45**, 224-228, doi:10.1006/geno.1997.4922 (1997).
42 Qian, Z., Okuhara, D., Abe, M. K. & Rosner, M. R. Molecular cloning and characterization of a mitogen-activated protein kinase-associated intracellular chloride channel. *J Biol Chem* **274**, 1621-1627, doi:10.1074/jbc.274.3.1621 (1999).
43 Duncan, R. R., Westwood, P. K., Boyd, A. & Ashley, R. H. Rat brain p64H1, expression of a new member of the p64 chloride channel protein family in endoplasmic reticulum. *J Biol Chem* **272**, 23880-23886, doi:10.1074/jbc.272.38.23880 (1997).
44 Berryman, M. & Bretscher, A. Identification of a novel member of the chloride intracellular channel gene family (CLIC5) that associates with the actin cytoskeleton of placental microvilli. *Mol Biol Cell* **11**, 1509-1521, doi:10.1091/mbc.11.5.1509 (2000).
45 Nishizawa, T., Nagao, T., Iwatsubo, T., Forte, J. G. & Urushidani, T. Molecular cloning and characterization of a novel chloride intracellular channel-related protein, parchorin, expressed in water-secreting cells. *J Biol Chem* **275**, 11164-11173, doi:10.1074/jbc.275.15.11164 (2000).
46 Littler, D. R. *et al.* The enigma of the CLIC proteins: Ion channels, redox proteins, enzymes, scaffolding proteins? *FEBS Lett* **584**, 2093-2101, doi:10.1016/j.febslet.2010.01.027 (2010).
47 Singh, H. & Ashley, R. H. CLIC4 (p64H1) and its putative transmembrane domain form poorly selective, redox-regulated ion channels. *Mol Membr Biol* **24**, 41-52, doi:10.1080/09687860600927907 (2007).
48 Al Khamici, H. *et al.* Members of the chloride intracellular ion channel protein family demonstrate glutaredoxin-like enzymatic activity. *PLoS One* **10**, e115699, doi:10.1371/journal.pone.0115699 (2015).
49 Fernandez-Salas, E. *et al.* mtCLIC/CLIC4, an organellular chloride channel protein, is increased by DNA damage and participates in the apoptotic response to p53. *Mol Cell Biol* **22**, 3610-3620, doi:10.1128/MCB.22.11.3610-3620.2002 (2002).
50 Tonini, R. *et al.* Functional characterization of the NCC27 nuclear protein in stable transfected CHO-K1 cells. *FASEB J* **14**, 1171-1178, doi:10.1096/fasebj.14.9.1171 (2000).
51 Valenzuela, S. M. *et al.* The nuclear chloride ion channel NCC27 is involved in regulation of the cell cycle. *J Physiol* **529 Pt 3**, 541-552, doi:10.1111/j.1469-7793.2000.00541.x (2000).
52 Tulk, B. M., Kapadia, S. & Edwards, J. C. CLIC1 inserts from the aqueous phase into phospholipid membranes, where it functions as an anion channel. *Am J Physiol Cell Physiol* **282**, C1103-1112, doi:10.1152/ajpcell.00402.2001 (2002).
53 Littler, D. R. *et al.* The intracellular chloride ion channel protein CLIC1 undergoes a redox-controlled structural transition. *J Biol Chem* **279**, 9298-9305, doi:10.1074/jbc.M308444200 (2004).
54 Harrop, S. J. *et al.* Crystal structure of a soluble form of the intracellular chloride ion channel CLIC1 (NCC27) at 1.4-A resolution. *J Biol Chem* **276**, 44993-45000, doi:10.1074/jbc.M107804200 (2001).
55 Averaimo, S., Milton, R. H., Duchen, M. R. & Mazzanti, M. Chloride intracellular channel 1 (CLIC1): Sensor and effector during oxidative stress. *FEBS Lett* **584**, 2076-2084, doi:10.1016/j.febslet.2010.02.073 (2010).
56 Goodchild, S. C. *et al.* Oxidation promotes insertion of the CLIC1 chloride intracellular channel into the membrane. *Eur Biophys J* **39**, 129-138, doi:10.1007/s00249-009-0450-0 (2009).
57 Kang, M. K. & Kang, S. K. Pharmacologic blockade of chloride channel synergistically enhances apoptosis of chemotherapeutic drug-resistant cancer stem cells. *Biochem Biophys Res Commun* **373**, 539-544, doi:10.1016/j.bbrc.2008.06.070 (2008).

58 Wang, L. *et al.* Elevated expression of chloride intracellular channel 1 is correlated with poor prognosis in human gliomas. *J Exp Clin Cancer Res* **31**, 44, doi:10.1186/1756-9966-31-44 (2012).
59 Wang, P. *et al.* Regulation of colon cancer cell migration and invasion by CLIC1-mediated RVD. *Mol Cell Biochem* **365**, 313-321, doi:10.1007/s11010-012-1271-5 (2012).
60 Cianci, F. & Verduci, I. Transmembrane Chloride Intracellular Channel 1 (tmCLIC1) as a Potential Biomarker for Personalized Medicine. *J Pers Med* **11**, doi:10.3390/jpm11070635 (2021).
61 Milton, R. H. *et al.* CLIC1 function is required for beta-amyloid-induced generation of reactive oxygen species by microglia. *J Neurosci* **28**, 11488-11499, doi:10.1523/JNEUROSCI.2431-08.2008 (2008).
62 Peretti, M. *et al.* Mutual Influence of ROS, pH, and CLIC1 Membrane Protein in the Regulation of G1-S Phase Progression in Human Glioblastoma Stem Cells. *Mol Cancer Ther* **17**, 2451-2461, doi:10.1158/1535-7163.MCT-17-1223 (2018).
63 Forman, H. J., Ursini, F. & Maiorino, M. An overview of mechanisms of redox signaling. *J Mol Cell Cardiol* **73**, 2-9, doi:10.1016/j.yjmcc.2014.01.018 (2014).
64 Bedard, K. & Krause, K. H. The NOX family of ROS-generating NADPH oxidases: physiology and pathophysiology. *Physiol Rev* **87**, 245-313, doi:10.1152/physrev.00044.2005 (2007).
65 Fiorani, M., Guidarelli, A. & Cantoni, O. Mitochondrial reactive oxygen species: the effects of mitochondrial ascorbic acid vs untargeted and mitochondria-targeted antioxidants. *Int J Radiat Biol* **97**, 1055-1062, doi:10.1080/09553002.2020.1721604 (2021).
66 Aggarwal, V. *et al.* Role of Reactive Oxygen Species in Cancer Progression: Molecular Mechanisms and Recent Advancements. *Biomolecules* **9**, doi:10.3390/biom9110735 (2019).
67 Storz, P. Reactive oxygen species in tumor progression. *Front Biosci* **10**, 1881-1896, doi:10.2741/1667 (2005).
68 Nishikawa, M. Reactive oxygen species in tumor metastasis. *Cancer Lett* **266**, 53-59, doi:10.1016/j.canlet.2008.02.031 (2008).
69 Hurd, T. R., DeGennaro, M. & Lehmann, R. Redox regulation of cell migration and adhesion. *Trends Cell Biol* **22**, 107-115, doi:10.1016/j.tcb.2011.11.002 (2012).
70 Chiarugi, P. & Fiaschi, T. Redox signalling in anchorage-dependent cell growth. *Cell Signal* **19**, 672-682, doi:10.1016/j.cellsig.2006.11.009 (2007).
71 Ushio-Fukai, M. & Urao, N. Novel role of NADPH oxidase in angiogenesis and stem/progenitor cell function. *Antioxid Redox Signal* **11**, 2517-2533, doi:10.1089/ARS.2009.2582 (2009).
72 Kheradmand, F., Werner, E., Tremble, P., Symons, M. & Werb, Z. Role of Rac1 and oxygen radicals in collagenase-1 expression induced by cell shape change. *Science* **280**, 898-902, doi:10.1126/science.280.5365.898 (1998).
73 Vesentini, N. *et al.* Modulation of erythrocyte sensitivity to oxidative stress by transient hyperhomocysteinemia in healthy subjects and in patients with coronary artery disease. *Nutr Metab Cardiovasc Dis* **18**, 402-407, doi:10.1016/j.numecd.2007.03.009 (2008).
74 Werner, E. & Werb, Z. Integrins engage mitochondrial function for signal transduction by a mechanism dependent on Rho GTPases. *J Cell Biol* **158**, 357-368, doi:10.1083/jcb.200111028 (2002).
75 Inumaru, J. *et al.* Molecular mechanisms regulating dissociation of cell-cell junction of epithelial cells by oxidative stress. *Genes Cells* **14**, 703-716, doi:10.1111/j.1365-2443.2009.01303.x (2009).

76 Lin, M. T., Yen, M. L., Lin, C. Y. & Kuo, M. L. Inhibition of vascular endothelial growth factor-induced angiogenesis by resveratrol through interruption of Src-dependent vascular endothelial cadherin tyrosine phosphorylation. *Mol Pharmacol* **64**, 1029-1036, doi:10.1124/mol.64.5.1029 (2003).
77 Kim, K. H. *et al.* Pro-MMP-2 activation by the PPARgamma agonist, ciglitazone, induces cell invasion through the generation of ROS and the activation of ERK. *FEBS Lett* **581**, 3303-3310, doi:10.1016/j.febslet.2007.06.012 (2007).
78 Nelson, K. K. & Melendez, J. A. Mitochondrial redox control of matrix metalloproteinases. *Free Radic Biol Med* **37**, 768-784, doi:10.1016/j.freeradbiomed.2004.06.008 (2004).
79 Tobar, N., Villar, V. & Santibanez, J. F. ROS-NFkappaB mediates TGF-beta1-induced expression of urokinase-type plasminogen activator, matrix metalloproteinase-9 and cell invasion. *Mol Cell Biochem* **340**, 195-202, doi:10.1007/s11010-010-0418-5 (2010).
80 Curran, S. *et al.* Matrix metalloproteinase/tissue inhibitors of matrix metalloproteinase phenotype identifies poor prognosis colorectal cancers. *Clin Cancer Res* **10**, 8229-8234, doi:10.1158/1078-0432.CCR-04-0424 (2004).
81 Lukaszewicz-Zajac, M., Mroczko, B. & Szmitkowski, M. Gastric cancer - The role of matrix metalloproteinases in tumor progression. *Clin Chim Acta* **412**, 1725-1730, doi:10.1016/j.cca.2011.06.003 (2011).
82 Brenneisen, P. *et al.* Activation of protein kinase CK2 is an early step in the ultraviolet B-mediated increase in interstitial collagenase (matrix metalloproteinase-1; MMP-1) and stromelysin-1 (MMP-3) protein levels in human dermal fibroblasts. *Biochem J* **365**, 31-40, doi:10.1042/BJ20020110 (2002).
83 Pelicano, H. *et al.* Mitochondrial dysfunction and reactive oxygen species imbalance promote breast cancer cell motility through a CXCL14-mediated mechanism. *Cancer Res* **69**, 2375-2383, doi:10.1158/0008-5472.CAN-08-3359 (2009).
84 Binker, M. G., Binker-Cosen, A. A., Richards, D., Oliver, B. & Cosen-Binker, L. I. EGF promotes invasion by PANC-1 cells through Rac1/ROS-dependent secretion and activation of MMP-2. *Biochem Biophys Res Commun* **379**, 445-450, doi:10.1016/j.bbrc.2008.12.080 (2009).
85 Cannito, S. *et al.* Redox mechanisms switch on hypoxia-dependent epithelial-mesenchymal transition in cancer cells. *Carcinogenesis* **29**, 2267-2278, doi:10.1093/carcin/bgn216 (2008).
86 Cannito, S. *et al.* Epithelial-mesenchymal transition: from molecular mechanisms, redox regulation to implications in human health and disease. *Antioxid Redox Signal* **12**, 1383-1430, doi:10.1089/ars.2009.2737 (2010).
87 Dong, J. J. *et al.* [Distribution of polymorphism in endothelial nitric oxide synthase gene in Singapore Chinese and its association with diabetic nephropathy]. *Zhonghua Yi Xue Za Zhi* **87**, 3415-3417 (2007).
88 Piskounova, E. *et al.* Oxidative stress inhibits distant metastasis by human melanoma cells. *Nature* **527**, 186-191, doi:10.1038/nature15726 (2015).
89 Le Gal, K. *et al.* Antioxidants can increase melanoma metastasis in mice. *Sci Transl Med* **7**, 308re308, doi:10.1126/scitranslmed.aad3740 (2015).
90 Peiris-Pages, M., Martinez-Outschoorn, U. E., Sotgia, F. & Lisanti, M. P. Metastasis and Oxidative Stress: Are Antioxidants a Metabolic Driver of Progression? *Cell Metab* **22**, 956-958, doi:10.1016/j.cmet.2015.11.008 (2015).
91 Nicoli S, Presta M. The zebrafish/tumor xenograft angiogenesis assay. Nat Protoc. 2007;2(11):2918-23. doi: 10.1038/nprot.2007.412. PMID: 18007628.
92 Lu, J., Dong, Q., Zhang, B. *et al.* Chloride intracellular channel 1 (CLIC1) is activated and functions as an oncogene in pancreatic cancer. *Med Oncol* **32,** 171 (2015).

93 Lee, JR., Lee, JY., Kim, HJ. *et al.* The inhibition of chloride intracellular channel 1 enhances Ca^{2+} and reactive oxygen species signaling in A549 human lung cancer cells.*Exp Mol Med* **51,** 1–11 (2019).

94 Yu W, Cui R, Qu H, Liu C, Deng H and Zhang Z: Expression and prognostic value of CLIC1 in epithelial ovarian cancer. Exp Ther Med **15**: 4943-4949, 2018

95 Anderson KJ, Cormier RT, Scott PM. Role of ion channels in gastrointestinal cancer. World JGastroenterol 2019; **25**(38):5732-5772

96 Meng M, Wang HB, Song SZ, Sun R, Lin Y, Lin S. CLIC1 facilitates cancer associated fibroblast activation and gastric cancer progression via integrins/NF-κB pathway. *Am J Physiol Gastrointest Liver Physiol*. 2020. First published Nov 11, 2020.

97 Acharya A, Das I, Chandhok D, Saha T. Redox regulation in cancer: a double-edged sword with therapeutic potential. Oxid Med Cell Longev. 2010 Jan-Feb;**3**(1):23-34.